Defense Nuclear Agency
Alexandria, VA 22310-3398

DNA-TR-90-78

Impact of Ionospheric Scintillations on Space-Based Surveillance Radars

Lester L. DeRaad, Jr.
Brian Lamb
R & D Associates
P.O. Box 92500
Los Angeles, CA 90009

June 1991

Technical Report

CONTRACT No. DNA 001-88-C-0046

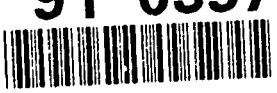

Destroy this report when it is no longer needed. Do not return to sender.

PLEASE NOTIFY THE DEFENSE NUCLEAR AGENCY, ATTN: CSTI, 6801 TELEGRAPH ROAD, ALEXANDRIA, VA 22310-3398, IF YOUR ADDRESS IS INCORRECT, IF YOU WISH IT DELETED FROM THE DISTRIBUTION LIST, OR IF THE ADDRESSEE IS NO LONGER EMPLOYED BY YOUR ORGANIZATION.

DISTRIBUTION LIST UPDATE

This mailer is provid ‹ to enable DNA to maintain current distribution lists for reports. We would appreciate your providing the requested information

☐ Add the individual listed to your distribution list.

☐ Delete the cited organization/individual.

☐ Change of address.

NOTE:
Please return the mailing label from the document so that any additions, changes, corrections or deletions can be made more easily.

NAME: _____

ORGANIZATION: _____

OLD ADDRESS	CURRENT ADDRESS
_____	_____
_____	_____
_____	_____

TELEPHONE NUMBER ( ) _____

SUBJECT AREA(s) OF INTEREST:

_____	_____
_____	_____
_____	_____

DNA OR OTHER GOVERNMENT CONTRACT NUMBER: _____

CERTIFICATION OF NEED-TO-KNOW BY GOVERNMENT SPONSOR (if other than DNA):

SPONSORING ORGANIZATION: _____

CONTRACTING OFFICER OR REPRESENTATIVE: _____

SIGNATURE _____

CUT HERE AND RETURN

Director
Defense Nuclear Agency
ATTN: TITL
Washington, DC 20305-[illegible]

Director
Defense Nuclear Agency
ATTN: TITL
Washington, DC 20305-1000

REPORT DOCUMENTATION PAGE

Form Approved OMB No. 0704-0188

1 AGENCY USE ONLY (Leave blank)	2 REPORT DATE	3. REPORT TYPE AND DATES COVERED
	910601	Technical 890103 – 891231

4. TITLE AND SUBTITLE

Impact of Ionospheric Scintillations on Space-Based Surveillance Radars

5 FUNDING NUMBERS

C - DNA 001-88-C-0046
PE - 62715H
PR - RD
TA - RC
WU - DH041780

6. AUTHOR(S)

Lester L. DeRaad, Jr., and Brian Lamb

7 PERFORMING ORGANIZATION NAME(S) AND ADDRESS(ES)

R & D Associates
P.O. Box 92500
Los Angeles, CA 90009

8 PERFORMING ORGANIZATION REPORT NUMBER

RDA-TR-161603-001

9 SPONSORING/MONITORING AGENCY NAME(S) AND ADDRESS(ES)

Defense Nuclear Agency
6801 Telegraph Road
Alexandria, VA 22310-3398
RAAE/Ullrich

10 SPONSORING/MONITORING AGENCY REPORT NUMBER

DNA-TR-90-78

11. SUPPLEMENTARY NOTES

This work was sponsored by the Defense Nuclear Agency under RDT&E RMC Code B4662D RD RC 00021 DFPR 1910A 25904D.

12a. DISTRIBUTION/AVAILABILITY STATEMENT

Approved for public release; distribution is unlimited.

12b DISTRIBUTION CODE

13. ABSTRACT *(Maximum 200 words)*

A model is developed to analyze propagation effects on space-based radars (SBRs) with pulse-Doppler processing and with a displaced phase center antenna (DPCA) for rejection of surface clutter. It is found that nuclear-disturbed ionospheric effects can significantly affect radar performance. Depending on the radar design parameters, similar, but less severe, problems may also occur in ambient auroral and equatorial ionospheres. The ionospheric effects degrade the DPCA clutter rejection and target Doppler processing functions of the radar.

14. SUBJECT TERMS		15. NUMBER OF PAGES
Space-Based Radar Propagation Effects	Rayleigh Fading Scintillation Effects	70
		16 PRICE CODE

17 SECURITY CLASSIFICATION OF REPORT	18 SECURITY CLASSIFICATION OF THIS PAGE	19. SECURITY CLASSIFICATION OF ABSTRACT	20 LIMITATION OF ABSTRACT
UNCLASSIFIED	UNCLASSIFIED	UNCLASSIFIED	SAR

CLASSIFIED BY:

N/A since Unclassified

DECLASSIFY ON:

N/A since Unclassified

SUMMARY

The primary result of this study is a comprehensive model for propagation effects on a space-based surveillance radar (SBR). Although the model is applicable to both Rayleigh and non-Rayleigh propagation conditions, analytic results are possible only for Rayleigh scintillation. Phase screen calculations are required for simulation of weak scintillation.

This report analyzes several candidate pulse-Doppler SBR systems in a target search mode. These candidate systems are analyzed primarily to illustrate the manner in which the model is utilized; hence the choice of SBR parameters may not represent the choice of SBRs currently under consideration for future deployment. Although the basic model of the DPCA and Doppler processing is applicable to any mode, this study does not attempt to quantify the affect of propagation effects on the angle tracking and range tracking loops required in a target track mode.

It is found that ionospheric propagation effects following a high-altitude nuclear explosion (HANE) can significantly degrade radar target detection performance. Depending on the radar design parameters, similar, but less severe performance degradation may occur in ambient auroral and equatorial ionospheres.

CONVERSION TABLE

Conversion factors for U.S. Customary to metric (SI) units of measurement.

MULTIPLY → BY → TO GET
TO GET ← BY ← DIVIDE

angstrom	1.000 000 X E -10	meters (m)
atmosphere (normal)	1.013 25 X E +2	kilo pascal (kPa)
bar	1.000 000 X E +2	kilo pascal (kPa)
barn	1.000 000 X E -28	meter^2 (m^2)
British thermal unit (thermochemical)	1.054 350 X E +3	joule (J)
calorie (thermochemical)	4.184 000	joule (J)
cal (thermochemical)/cm^2	4.184 000 X E -2	mega joule/m^2 (MJ/m^2)
curie	3.700 000 X E +1	giga becquerel (GBq)*
degree (angle)	1.745 329 X E -2	radian (rad)
degree Fahrenheit	$T_K=(t°f+459.67)/1.8$	degree kelvin (K)
electron volt	1.602 19 X E -19	joule (J)
erg	1.000 000 X E -7	joule (J)
erg/second	1.000 000 X E -7	watt (W)
foot	3.048 000 X E -1	meter (m)
foot-pound-force	1.355 818	joule (J)
gallon (U.S. liquid)	3.785 412 X E -3	meter^3 (m^3)
inch	2.540 000 X E -2	meter (m)
jerk	1.000 000 X E +9	joule (J)
joule/kilogram (J/kg) (radiation dose absorbed)	1.000 000	Gray (Gy)**
kilotons	4.183	terajoules
kip (1000 lbf)	4.448 222 X E +3	newton (N)
kip/inch^2 (ksi)	6.894 757 X E +3	kilo pascal (kPa)
ktap	1.000 000 X E +2	newton-second/m^2 (N-s/m^2)
micron	1.000 000 X E -6	meter (m)
mil	2.540 000 X E -5	meter (m)
mile (international)	1.609 344 X E +3	meter (m)
ounce	2.834 952 X E -2	kilogram (kg)
pound-force (lbf avoirdupois)	4.448 222	newton (N)
pound-force inch	1.129 848 X E -1	newton-meter (N·m)
pound-force/inch	1.751 268 X E +2	newton/meter (N/m)
pound-force/foot^2	4.788 026 X E -2	kilo pascal (kPa)
pound-force/inch^2 (psi)	6.894 757	kilo pascal (kPa)
pound-mass (lbm avoirdupois)	4.535 924 X E -1	kilogram (kg)
pound-mass-foot^2 (moment of inertia)	4.214 011 X E -2	kilogram-meter^2 (kg·m^2)
pound-mass/foot^3	1.601 846 X E +1	kilogram/meter^3 (kg/m^3)
rad (radiation dose absorbed)	1.000 000 X E -2	Gray (Gy)**
roentgen	2.579 760 X E -4	coulomb/kilogram (C/kg)
shake	1.000 000 X E -8	second (s)
slug	1.459 390 X E +1	kilogram (kg)
torr (mm Hg, 0°C)	1.333 22 X E -1	kilo pascal (kPa)

* The becquerel (Bq) is the SI unit of radioactivity; 1 Bq = 1 event/s.
**The Gray (Gy) is the SI unit of absorbed radiation.

TABLE OF CONTENTS

LIST OF ILLUSTRATIONS

LIST OF ILLUSTRATIONS (Concluded)

SECTION 1
INTRODUCTION

A constellation of space-based radars (SBRs) has been under consideration as a candidate for the broad area surveillance and target tracking required in future air defense missions. These missions require the detection and tracking of aircraft and/or cruise missiles that could threaten naval battle groups and the continental United States (CONUS). Several different combinations of missions and threats have been considered in system architecture studies. Studies of the fleet defense mission consider long range bombers as the primary threat whereas studies of strategic air defense of CONUS consider a combined threat consisting of bombers, air-launched cruise missiles (ALCMs) and sea-launched cruise missiles (SLCMs).

The radar propagation path must traverse the ionosphere. It is known that ionospheric disturbances can cause disruption of transionospheric radio wave propagation (Refs. 1-16). Ambient high-altitude and equatorial region ionospheric disturbances often cause severe amplitude and phase scintillation of VHF signals (Refs. 2-5 and 7-11). Scintillation of signals at frequencies up to L band is commonly observed in the equatorial region due to a severe ionospheric disturbance known as equatorial spread F (Refs. 2,4-7 and 12-14). Phase scintillation of L-band signals is also occasionally observed in high-latitude regions due to naturally occurring disturbances (Ref. 3). In addition, very severe scintillation will result at frequencies up to EHF for propagation through the disturbed ionospheric environment occurring following a high-altitude nuclear explosion (HANE) (Refs. 17-26).

Ionospheric scintillation effects decrease with decreasing radar wavelength, whereas the cross section of cruise missiles tend to increase with increasing wavelength. Although a UHF space-based radar has been proposed as a compromise between these two trends, this paper analyzes the effect of a disturbed propagation environment on VHF, UHF, and L-band surveillance radar systems.

Since the antenna footprint is many orders of magnitude larger than the size of targets, the backscattered signal will be dominated by the contribution from surface clutter. Doppler processing to discriminate between targets and clutter is complicated by the large Doppler

shift of the clutter signal due to the large platform velocity of a SBR. Use of a displaced phase center antenna (DPCA) may be required at long radar wavelengths (due to the extremely large antenna footprints) in order to achieve the level of clutter rejection necessary for target detection.

Propagation effects can degrade the performance of a space-based surveillance radar in several ways (Refs. 27-30). Amplitude fading can reduce the probability of detection. In addition, phase scintillation can spread the Doppler spectrum of a target return signal beyond the Doppler resolution of the radar; this reduces the ratio of target signal to clutter signal and/or noise with a resulting reduction in probability of detection. There is also a reduction in radar antenna gain and an increase in beamwidth caused by a loss of signal coherence along the antenna aperture. Finally, propagation effects can cause a marked reduction in the clutter rejection performance of the DPCA.

The report is organized as follows. Section 2 gives a brief qualitative description of the operation of the DPCA, derives the radar equation for detection of a target in clutter, and demonstrates why the use of a DPCA is often proposed for a low-altitude UHF surveillance radar. The derivation of the radar equation includes the effects of propagation through the disturbed environment following a HANE event. Section 3 gives examples of the effects of disturbed propagation environments upon low-altitude UHF and L-band surveillance radars, while Section 4 contains some concluding remarks. An analysis of propagation effects on DPCA clutter rejection performance and scintillation-induced Doppler broadening of the radar signal is given in Appendix A. Details of the propagation environment are given in Appendix B.

SECTION 2
INTRODUCTION TO THE MODEL

This section introduces the model and illustrates the operation of pulse-Doppler space-based surveillance radars through a derivation of the radar equation for target detection. In order to make the discussion of this section more concrete, specific parameters for a UHF SBR are used in the illustrations. The formalism for treating the impact of propagation effects on the signal-to-clutter ratio is introduced.

Targets must be detected in the presence of large surface clutter returns. An equation for the target signal-to-clutter power ratio is derived; this radar equation includes the effects of propagation through a disturbed ionospheric environment. It is demonstrated that a displaced phase center antenna (DPCA) is often recommended for a low-altitude UHF surveillance radar under undisturbed propagation conditions to reduce the clutter amplitude to acceptable levels.

The effect of propagation through a disturbed ionospheric environment enters the radar equation in several ways; the DPCA clutter rejection performance is reduced, the target signal is Doppler spread and/or Doppler shifted, the antenna gain is reduced, and the antenna beam is broadened resulting in a larger clutter cross section and Doppler bandwidth.

The displaced phase center antenna (DPCA) is used to reject the signal due to stationary surface clutter. This is accomplished by dividing the antenna into several subapertures with phase centers that are physically separated. Through a combination of space and time diversity, the return signal from surface clutter is rejected. This technique enables detection of moving targets with radar returns that are several orders of magnitude weaker than surface clutter.

The simplest implementation of DPCA, which we call two phase center DPCA, is shown in Figure 1. There, for simplicity, we show two separate antennas whereas actually a single antenna is used with phase centers that are electronically adjustable. The operation is as follows. At some time, say $t = 0$, a pulse is transmitted from the front antenna. This signal propagates to the targets and clutter, is scattered, and propagates back to the radar platform. For a space-based system the signal round trip travel time t_d can be reasonably large, so the platform can move a considerable distance as shown in Figure 1. The scattered

signal is received by the front antenna. Due to platform motion, at some time $t = \Delta$ the rear antenna has moved into the same position that was occupied by the front antenna at $t = 0$. (The platform is now shown drawn in dashed lines.) Clearly, this time Δ is given by $\Delta = V/d$, where V is the velocity of the platform and d is the separation of the two phase centers. The rear antenna now emits a signal which propagates, scatters, and propagates back to the platform to be received by the rear antenna. As shown in Figure 1, at time $t = t_d + \Delta$ the rear antenna has moved into the position that the front antenna occupied when it received a signal at time $t = t_d$. For a stationary patch of clutter, it is evident that the two ray paths are identical, and hence the clutter contributions to the two received signals will be identical. The clutter contributions of these two signals will cancel when the signals are subtracted. On the other hand, the signal round trip time for a moving target will be different from the two pulses, hence there will be a residual when the signals are subtracted.

There are a number of disadvantages to the two phase center approach described in Figure 1. In particular, the pulse repetition frequency (PRF) out of the two pulse canceller is one-half the PRF of the transmitted waveform. In fact, the usually recommended implementation for both airborne and space-borne DPCA systems is a three phase center approach. The three phase center DPCA enjoys the advantage that it can be implemented using the sum and difference channels of a monopulse radar antenna.

The three phase center implementation is shown in Figure 2. It operates as follows. At time $t = 0$ a signal is transmitted employing the entire aperture with its phase center at the center of the antenna. The signal propagates to the clutter and targets, is scattered, and propagates back to the radar platform. Upon reception at time $t = t_d$, the antenna is configured to have two phase centers (forward and rear) that both receive the signal. At time $t = \Delta$, the platform has moved such that the center phase center is located at the position that the front phase center occupied on the previous pulse. (The platform is now shown drawn in dashed lines.) We have the relation $\Delta = d/2V$, where d is the separation between the front and rear phase centers. This second pulse is transmitted and eventually received at time $t = t_d + \Delta$ by both the forward and rear phase centers. Between pulses, the phase centers have advanced a distance $d/2$. The signal received by the forward phase center for the first pulse (solid line) and by the rear phase center for the second pulse (dashed line) are shown in Figure 2. The difference signal between these two signals is taken. This procedure will null returns from stationary objects. Cancellation of the difference signal from stationary clutter occurs because the two-way propagation path

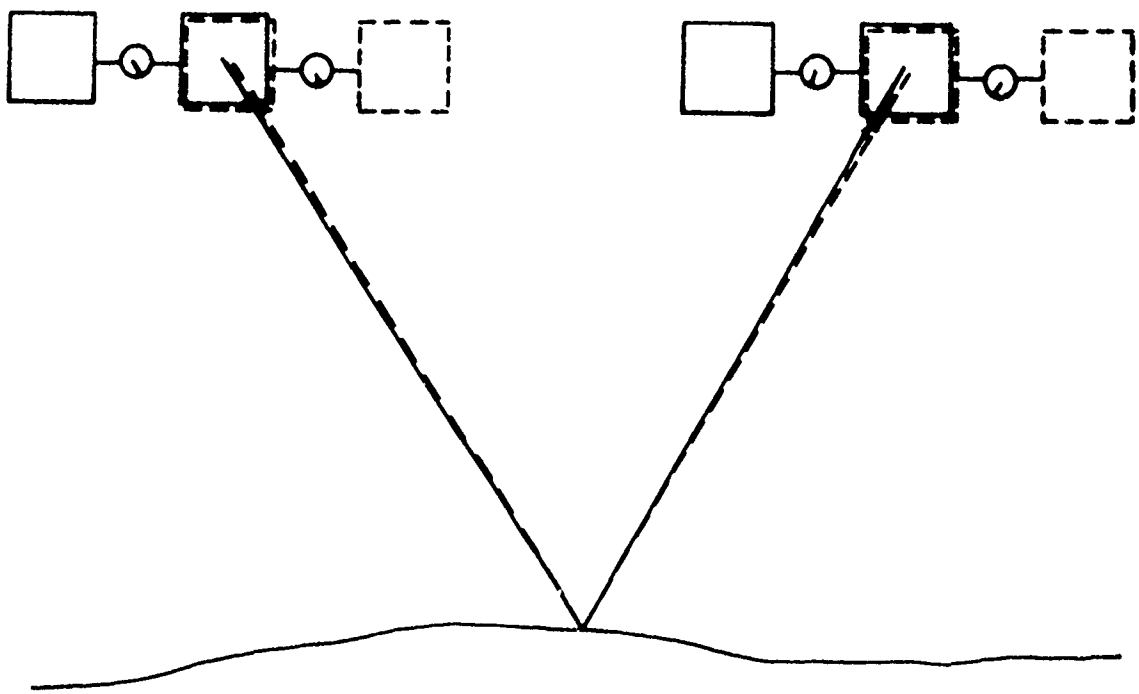

Figure 1. Two phase center DPCA operation. The solid line is the first pulse and the dashed line is the second pulse. Platform motion is to the right.

lengths coincide to a high degree of accuracy. Alternatively, the two-way propagation path lengths to a moving target will not coincide.

Clutter cancellation will be impaired if the characteristics of the DPCA propagation paths vary between radar pulses as can occur if the radar line-of-sight passes through structured ionospheric plasma. The two implementations of DPCA are affected differently by propagation effects. Although the propagation paths used in the two phase center DPCA physically coincide, they are separated in time by the amount Δ. Hence, a time evolution of the ionospheric plasma, as occurs when there is a bulk plasma drift across the line-of-sight, can introduce different phase shifts into the two propagation paths. Even if Δ is a small fraction of the signal decorrelation time, there can be a substantial reduction in the

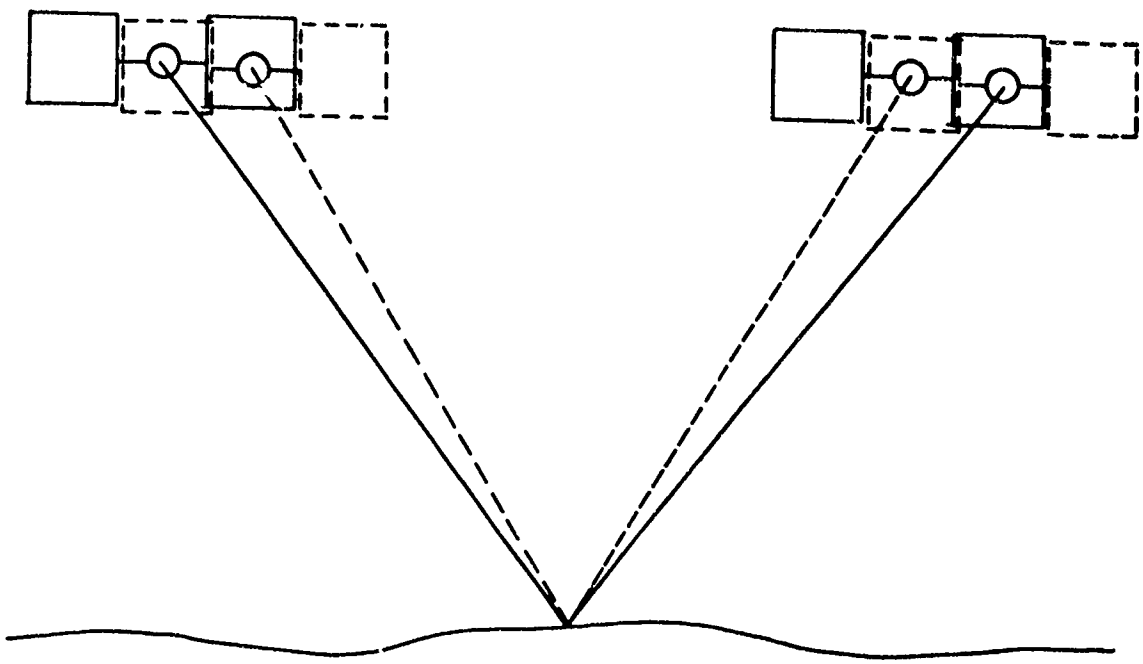

Figure 2. Three phase center DPCA operation: The solid line is the first pulse and the dashed line is the second pulse. Platform motion is to the right.

clutter rejection performance, with a consequent reduction in signal-to-clutter ratio. The propagation paths used in the three phase center DPCA differ in both space and time. Hence, structured ionospheric plasma can degrade DPCA performance even in the absence of a bulk plasma drift. If the path separation is a small fraction of the signal decorrelation length, a substantial reduction in clutter rejection performance can result.

Although the following radar equation is applicable to any space-based surveillance radar, for purposes of illustration, specific numbers will be evaluated for a generic UHF radar operating at 430 MHz, in a 355 nautical mile (650 km) circular orbit with an antenna

aperture measuring $D_{az} = 48$ m in the azimuth dimension (the antenna dimension parallel to the platform motion direction) and $D_{el} = 16$ m in the elevation dimension (the antenna dimension perpendicular to the platform motion direction). The radar waveform is assumed to have a bandwidth of 1 MHz and a pulse-repetition-frequency of 2000 Hz. Calculations will be performed for a line-of-sight grazing angle of $\alpha = 25°$. This is one of two systems for which more detailed results are given in Section 3.

The resulting antenna footprint measures

$$\Delta A = \left[\frac{\pi}{2\ell n 2}\right]^{\frac{1}{2}} \frac{R_0 \lambda}{2D_{az}}, \tag{1}$$

in the azimuth or along-track dimension by

$$\Delta R = \left[\frac{\pi}{2\ell n 2}\right]^{\frac{1}{2}} \frac{R_0 \lambda}{2D_{el} \sin\alpha} \tag{2}$$

in the range direction. In Eqs. 1 and 2, R_o is the slant range, λ is the radar signal wavelength, and α is the radar line-of-sight grazing angle. The footprint widths are computed by taking the 3-dB beamwidth (in the absence of propagation effects) to be $R_o\lambda/D$, fitting this 3-dB beamwidth to a Gaussian, and integrating over the two-way Gaussian beamwidth to find the effective beamwidth. The slant range is given by

$$R_0 = \left[R_e^2 \sin^2\alpha + h^2 + 2hR_e\right]^{\frac{1}{2}} - R_e \sin\alpha \tag{3}$$

where h is the radar platform altitude and R_e is the radius of the Earth. For the UHF radar mentioned above, $R_o = 1300$ km, $\Delta A = 14$ km and $\Delta R = 100$ km at a grazing angle of 25°.

As depicted in Figure 3, at small grazing angles such that the range ambiguity length $R_{\rm amb}$ is less than ΔR, surface clutter is received simultaneously from several ambiguous range swaths; the separation $R_{\rm amb}$ of the ambiguous range swaths depends on the interpulse period Δ through

$$R_{\rm amb} = \frac{c\Delta}{2\cos\alpha}, \tag{4}$$

where c is the velocity of light. The main-beam clutter cross section σ_c equals the clutter cross section per unit area, σ_o, multiplied by the area of the ambiguous range swaths lying within the antenna footprint. Thus we have

$$\sigma_c = n\sigma_0 \Delta A \Delta y, \tag{5}$$

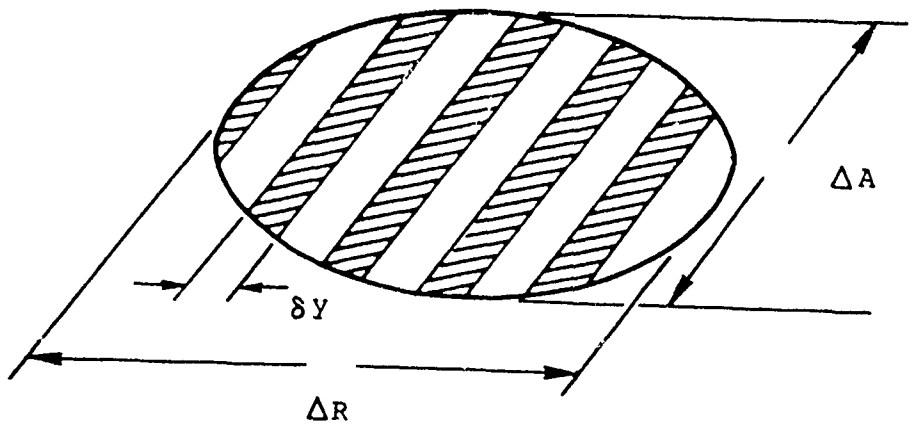

Figure 3. Antenna footprint with ambiguous range swaths hatched.

where n is the number of ambiguous range swaths and the ground range resolution Δy is given by

$$\Delta y = \frac{c}{2B\cos\alpha}. \tag{6}$$

In Eq. 6, B is the radar bandwidth (assumed to be 1 MHz for the UHF example). In the small grazing angle limit where $R_{amb} \ll \Delta R$, that is for

$$\tan\alpha \ll \left[\frac{\pi}{2\ell n2}\right]^{\frac{1}{2}} \frac{R_0\lambda}{cD_{el}\Delta}, \tag{7}$$

the number of ambiguous range swaths is given approximately by $\Delta R/R_{amb}$. Thus, for $R_{amb} < \Delta R$ the surface clutter cross section is approximately

$$\sigma_c \simeq \frac{\pi}{8\ell n2} \frac{\sigma_0\lambda^2 R_0^2}{D_{az}D_{el}\Delta\sin\alpha}. \tag{8}$$

Alternatively, when $R_{amb} > \Delta R$, there can be at most one clutter swath of width Δy so that

$$\sigma_c \simeq \left[\frac{\pi}{2\ell n2}\right]^{\frac{1}{2}} \frac{\sigma_c\lambda cR_0}{4D_{az}B\cos\alpha}. \tag{9}$$

A representative value of σ_o for land clutter at UHF, that will be exceeded 10 percent of the time, is -33 dB (Ref. 31). For a worst case we will take $\sigma_o = -20$ dB. For the UHF

radar example, Eq. 7 implies that the clutter cross section is given approximately by Eq. 9. Substitution of the UHF radar parameters into Eq. 9 and evaluating for a grazing angle of 25° gives

$$\sigma_c = 43.7 \text{ dB m}^2. \tag{10}$$

However, the clutter magnitude is significantly reduced through a combination of three methods; Doppler processing, antenna pattern rejection, and use of a DPCA.

As discussed previously, DPCA will be used to cancel the surface clutter signal. The amplitude and phase of the two signals that are differenced must be controlled to a high degree of accuracy. In order to maintain 40 dB of clutter cancellation the amplitude must be maintained to within 1 percent and the standard deviation of the phase error must be maintained to within 0.5 degrees. Furthermore, this accuracy must be maintained over the entire antenna pattern. Implementation of these hardware tolerances is very difficult to achieve, particularly in the sidelobes of the antenna. Hence, even in the absence of propagation effects, hardware tolerances will probably limit clutter cancellation to no better than 40 dB.

The DPCA residual clutter spectrum is schematically illustrated in Figure 4. Although ideal operation of the DPCA makes the radar platform look stationary, the residual clutter spectrum due to imperfect cancellation will have a spectrum similar to a non-DPCA antenna. The most obvious difference is that the residual sidelobe spectrum will be somewhat high relative to the residual mainlobe clutter due to difficulty in matching antenna sidelobes. The sidelobe clutter occurs between $-2V/\lambda$ and $+2V/\lambda$ in Doppler frequency (where V is the platform velocity) while the mainlobe clutter residual is centered at $(2V/\lambda)\cos\theta_a$ where θ_a is the angle between the antenna bore-sight and the platform velocity vector. (For the example UHF radar under discussion, θ_a is taken to be 90°.) When the antenna is pointed broadside, as in Figure 4, the mainlobe clutter residual is centered about zero frequency. In the general case there is also a large sidelobe return at zero frequency. This return, known as the altitude return, is due to the large specular clutter return coming from the region directly below the platform. It is masked by the mainlobe clutter when the antenna is pointed broadside. The width of the mainlobe clutter residual Δf_{cl} is (assuming a Gaussian antenna pattern, see Appendix A)

$$\Delta f_{cl} = \left[\frac{\pi}{2\ell n 2}\right]^{\frac{1}{2}} \frac{V}{D_{az}} \sin\theta_a. \tag{11}$$

The spectrum shown in Figure 4 is not strictly correct as it is the spectrum appropriate for a CW radar. In reality, the radar signal is modulated with a signal that typically consists of a pulse waveform that is repeated at one or more PRFs over a finite dwell time T_c. The spectrum of a typical modulation signal is shown in Figure 5. The spectrum consists of narrow spikes at the harmonics of the PRFs. The spikes have a width that is consistent with the attainable Doppler resolution ($1/T_c$). The amplitude of the spikes is modulated by the spectrum of a single pulse; hence, the overall bandwidth is the bandwidth of a single pulse.

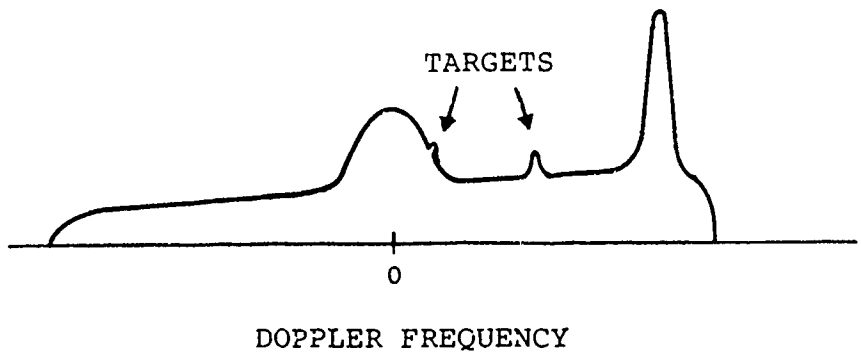

Figure 4. Doppler spectrum for CW radar.

The actual Doppler spectrum is the convolution of the modulation spectrum, Figure 5, with the spectrum for a CW radar, Figure 4. The primary effect of this convolution process is that the spectrum shown in Figure 4 is repeated at the harmonics of the PRF. With this in mind we return to our discussion of Figure 4.

Two target returns are shown in Figure 4 in addition to the residual clutter signal. In this example one target is in the mainlobe clutter region and another target is in the sidelobe clutter region. Since the sidelobe clutter is highly Doppler ambiguous for any practical PRF, sidelobe clutter will occupy all portions of the Doppler spectrum.

The radar uses two techniques to discriminate between various targets and clutter. At any given instant in time, as shown in Figure 3, the radar illuminates numerous range

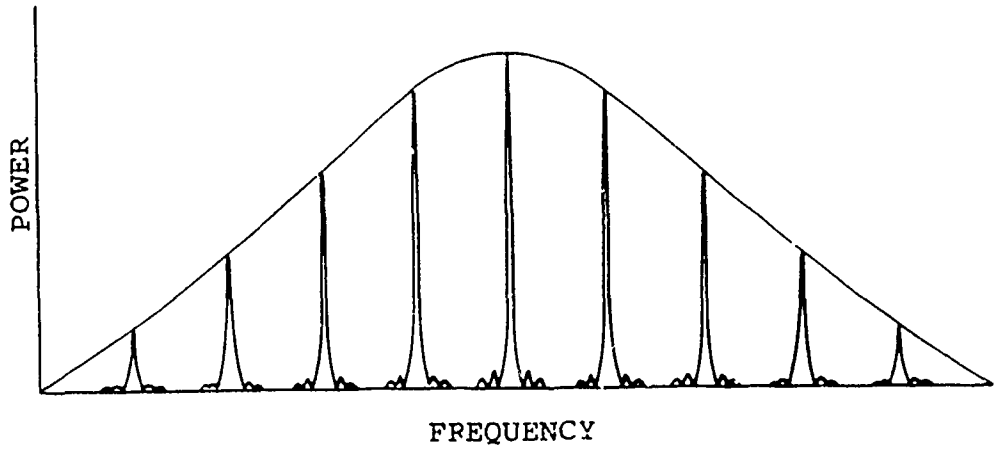

Figure 5. Modulation spectrum of pulse-Doppler radar.

ambiguous swaths in the antenna footprint. The received signal prior to range gating will contain contributions from all portions of the antenna footprint. Range gating selects one particular set of range ambiguous swaths. Hence, some targets may be isolated from others through range gating. The other discrimination technique is Doppler processing.

As illustrated in Figure 4, the clutter signal has a Doppler bandwidth Δf_{cl} that is considerably larger than the Doppler resolution Δf_D obtained through coherent processing; thus, only a small fraction of the total clutter signal energy will lie in a given Doppler bin. Coherent processing over a dwell time T_c yields a Doppler processing bandwidth Δf_D of

$$\Delta f_D = 1/T_c. \tag{12}$$

An improvement factor due to Doppler processing I_D can be defined as

$$I_D = \frac{\Delta f_{cl}}{\Delta f_D} = \left[\frac{\pi}{2\ell n 2}\right]^{\frac{1}{2}} \frac{VT_c}{D_{az}} \sin\theta_a. \tag{13}$$

Returning to the UHF radar example and using a typical coherent processing time of $T_c = 0.1$ sec and a platform velocity of $V = 7.5$ km/s, we find $\Delta f_{cl} = 235$ Hz, $\Delta f_D = 10$ Hz, and $I_D = 13.7$ dB.

Due to target motion, the Doppler shift of a target will usually differ from the center frequency of the clutter spectrum. As shown in Figure 6, if the antenna beamwidth is sufficiently narrow in azimuth, some clutter rejection will be obtained through antenna pattern rejection. This antenna pattern improvement factor I_A can be estimated, assuming a Gaussian antenna beam pattern and a sufficiently small target Doppler shift, through the factor (see Appendix A)

$$I_A = \exp \frac{\pi(2v_t/\lambda)^2}{\Delta f_{cl}^2} = \exp \frac{8\ell n 2 v_t^2 D_{az}^2}{V^2 \lambda^2}, \tag{14}$$

which represents the relative clutter amplitude evaluated at the Doppler frequency corresponding to a target with a velocity component along the radar line-of-sight of v_t. (Again, it is assumed that the antenna is pointing broadside.) Assuming a desired minimum-detectable velocity of 45 m/s and using this value for v_t in Eq. 14, gives $I_A = 4.1$ dB for the parameters of the UHF radar.

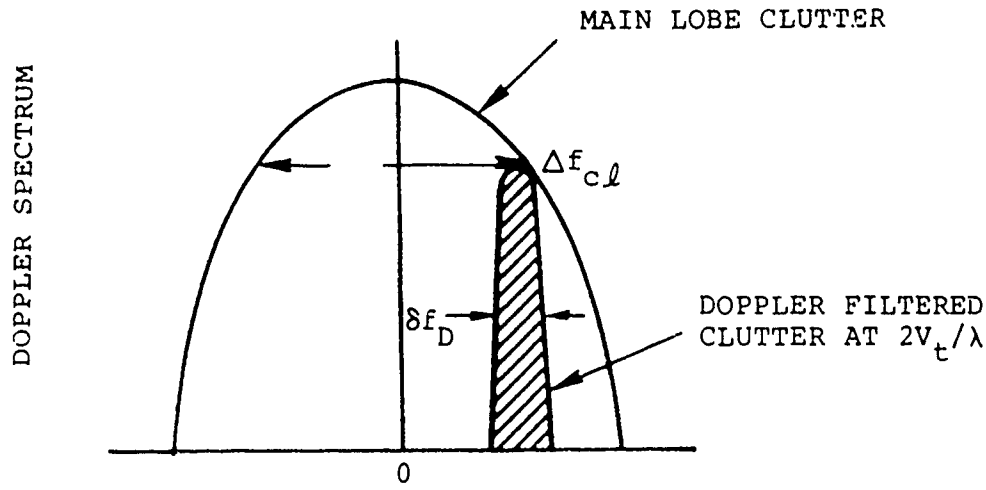

Figure 6. Clutter spectrum before and after Doppler filtering.

A radar equation for the signal-to-clutter ratio, S/C, can be written as

$$S/C = \frac{\langle \sigma_t \rangle I_D I_A I_{DPCA}}{\sigma_c L_B}, \tag{15}$$

where $\langle \sigma_t \rangle$ is the average target cross section, I_{DPCA} is the DPCA improvement factor and L_B, Eq. A65, is a target beam loss factor that accounts for targets that are not in the center of the antenna footprint. The signal-to-clutter ratio must be on the order of 10 to 15 dB for reliable target detection; the exact value will depend on the probabilities of detection and false alarm required, the statistics of cross section fluctuations, and the amount of incoherent averaging.

For the UHF system, requiring a signal-to-clutter ratio of at least 13 dB implies that 50 dB of DPCA improvement is required for detection of a 0.1 m^2 cross section target (assuming a minimum detectable velocity of 45 m/sec). Similarly, 40 dB of DPCA improvement is required for detection of a 1-m^2 cross section target. Noting that the DPCA improvement factor depends on target velocity (−5 dB for this example, Eq. A67a), the clutter rejections required are 55 dB and 45 dB, respectively.

Thus, good clutter rejection performance is a necessity for a UHF space-based surveillance radar system. The majority of clutter rejection is provided by the DPCA. System mismatches, such as imperfectly matched antenna patterns from the two displaced phase centers, place a finite limit on the clutter rejection performance of DPCA. Ionospheric induced propagation disturbances will further degrade DPCA performance as well as introduce a scintillation-induced loss caused by the Doppler spread of target returns. The remainder of this section introduces these effects into the radar equation for the signal-to-clutter ratio.

As shown in Appendix A, propagation disturbances place an upper limit on DPCA performance. The best achievable DPCA improvement factor I_{DPCA} for a situation in which the propagation path passes through an ionospheric propagation disturbance, reprinted here from Appendix A, is $I_{DPCA} = \Delta_T/\Delta_C$, where the difference signal for the target Δ_T is

$$\Delta_T = A - 2B\cos 2\bar{\alpha}, \tag{16}$$

and the difference signal for the clutter Δ_C is

$$\Delta_C = A - 2B\exp -\frac{\pi^2}{2\ell_a^2} S_{az} \left[\frac{S_{az}-1}{S_{az}}\right]^2 \left[\frac{V_p \Delta}{D_{az}}\right]^2. \tag{17}$$

For the two phase center implementation the A and B coefficients are

$$A_2 = 2\left(1 + \exp\left(-2t_d^2 V^2 / S_{az}\ell_o^2\right)\right) \tag{18a}$$

and

$$B_2 = \frac{1}{2} A_2 \exp - \frac{2\Delta^2}{S_{az} \ell_0^2} V_2^2. \tag{18b}$$

The antenna scatter coefficient S_{az} represents the reduction in antenna gain resulting from propagation effects and is defined through

$$S_{az} = 1 + \frac{4\ell n 2}{\pi^2} \frac{D_{az}^2}{\ell_0^2}, \tag{19}$$

in which ℓ_0 is the decorrelation length for one-way propagation evaluated at the radar platform altitude.

For the three center implementation the A and B coefficients are

$$A_3 = 2 + \exp\left[-2(t_d V + d/2)^2 / S_{az} \ell_0^2\right] + \exp\left[-2(t_d V - d/2)^2 / S_{az} \ell_0^2\right] \tag{20a}$$

and

$$B_3 = \exp\left[-\frac{2\Delta^2 V_2^2}{S_{az} \ell_0^2}\right] \left[\exp\left(-d^2 / 2 S_{az} \ell_0^2\right) + \exp\left(-2 t_d^2 V^2 / S_{az} \ell_0^2\right)\right] \tag{20b}$$

where

$$d = 2\Delta\left(V - v_{Ex}\right). \tag{20c}$$

The following symbols have also been defined:

$$\begin{aligned} \bar{\alpha} &= \frac{2\pi}{\lambda} \Delta \widehat{R}_0 \cdot \left[\mathbf{v}_0 + \frac{S_{az} - 1}{S_{az}} \left(v_{Ex} + \frac{R_+}{R_-} v_{Ex} + \frac{R_+}{R_-} v_{0x}\right) \mathbf{i}\right], \\ V_1 &= V + \frac{R_+}{R_-} v_x, \\ V_2 &= v_{Ex} + \frac{R_+}{R_-} v_x. \end{aligned} \tag{21}$$

We have specialized to a one-dimensional phase screen with variation and a possible drift motion along the platform motion direction (x direction). R_+ is the distance between the platform and the phase screen and R_- is the distance between the phase screen and the earth's surface. $\widehat{R}_o$ is a unit vector pointing from the antenna center to the target, V is the platform velocity relative to the phase screen (which is by assumption constrained to be in the x direction), $\mathbf{v}_E$ is the earth's velocity relative to the phase screen, $\mathbf{v}_0$ is the target velocity relative to the earth, and v_x represents either the x component of the earth velocity (when clutter is being considered) measured relative to the phase screen, or the x component of the target velocity measured relative to the phase screen. Hence, v_x represents v_{Ex} when clutter is being considered and $v_{Ex} + v_{0x}$ when the target is

being considered. Furthermore, we have specialized to the case where the antenna points broadside.

In addition to the degradation of DPCA performance, propagation induced scintillation causes an apparent Doppler spread and Doppler shift of the return signal. Although this effect occurs to both the surface clutter return and the return from a discrete target, the propagation induced Doppler spread and shift of the clutter is generally negligibly small compared to the main-beam clutter bandwidth Δf_{cl}. Alternatively, the Doppler shift and/or spread can be significant compared to the radar Doppler resolution Δf_D; the Doppler spread can spread the energy returned from a discrete target over a spectral width greater than Δf_D with a consequent decrease in signal-to-clutter ratio. In addition, a net propagation induced Doppler shift may cause the target to appear in the wrong Doppler bin. This may not be important if accurate target velocity information is not needed, as may be the case when the radar is in the search mode. Alternatively, if the net Doppler shift changes from scan to scan, and if some incoherent processing is performed, there may be a further performance reduction.

The performance reduction due to a Doppler spread is quantified through a coherent integration loss factor L_{ci}. When the scintillation induced Doppler spread Δf_{sc} is less than the radar Doppler resolution Δf_D, there is no loss,

$$L_{ci} = 1. \tag{22}$$

When $\Delta f_{sc} > \Delta f_D$, the coherent integration loss factor becomes

$$L_{ci} = \frac{\Delta f_{sc}}{\Delta f_D} = \Delta f_{sc} T_c. \tag{23}$$

If the Doppler spread is due primarily to multipath propagation, that is, when the contribution due to the phase-only effects can be neglected, the coherent integration loss from Appendix A becomes

$$L_{ci} = \left[1 + \frac{2}{\pi}\left[\frac{2V_1^2 T_c^2}{\pi S_{az} \ell_0^2}\right]^{\frac{1}{2}} + \frac{2V_1^2 T_c^2}{\pi S_{az} \ell_0^2}\right]^{\frac{1}{2}}. \tag{24}$$

We assume that the radar system will be designed such that under normal operating conditions, that is, in the absence of ionospheric induced propagation disturbances, the noise level will be greater than the clutter signal level at all Doppler frequencies of interest.

When a propagation disturbance occurs, the clutter signal level will increase to levels exceeding the noise level; under these disturbed conditions the detection performance is given in terms of the radar equation for the signal-to-clutter ratio S/C (Eq. A60),

$$\frac{S}{C} = \frac{\langle \sigma_t \rangle I_D I_A I_{\mathrm{DPCA}}}{\sigma_c L_{ci} I_B \sqrt{S_{az}}}. \tag{25}$$

Propagation effects will be investigated for candidate UHF and L-band systems in Section 3.

SECTION 3
PROPAGATION EFFECTS ON CANDIDATE SBR SYSTEMS

This section applies the space-based radar target detection model to candidate UHF and L-band pulse-Doppler surveillance radars. The degradation in signal-to-clutter ratio is quantified for propagation environments ranging from benign natural to post HANE environments. Performance of two phase center and three phase center DPCA implementations are contrasted.

The parameters of the candidate L-band and UHF systems are listed in Table 1. These candidate systems were analyzed primarily to illustrate the manner in which the model is utilized and uncover the relative sensitivity to propagation effects; hence the choice of SBR parameters may not represent the systems currently under consideration for future deployment.

Table 1. Parameters of the candidate space-based radar systems. The antenna aperture dimensions are listed with the along-track (or azimuth) dimension proceeding the cross-track (or elevation) dimension.

Parameter	L-band System	UHF System
Frequency	1.2 GHz	430 MHz
Altitude	650 km	650 km
PRF	5000 Hz	2000 Hz
Grazing Angle	25°	25°
Antenna Aperture	40 m × 15 m	48 m × 16 m
Radar Bandwidth	1 MHz	1 MHz
Integration Time	0.1 sec	0.1 sec
Target Cross Section	0 dBsm	0 dBsm
Clutter Reflectivity	−20 dB	−20 dB

An ionospheric striation drift velocity of 200 m/sec was assumed. Although the (circular) orbital velocity is 7.5 km/sec for the selected altitude, all velocities used in Section 2 and Appendix A are measured relative to the rest frame of the striations; hence, a platform velocity of $V = 7.3$ km/sec was taken. Depending on the orbital parameters and the radar look geometry, the velocity of the Earth's surface can range up to several hundred meters per second. A typical value (relative to the ionospheric striations) of $v_{Ex} = 200$ m/sec was taken.

Signal-to-clutter ratios depend strongly upon the target's velocity component along the radar line-of-sight. All calculations shown in this section were performed for a typical minimum detectable target velocity of $v_t = 45$ m/sec. Signal-to-clutter ratios were calculated versus decorrelation length ℓ_0 evaluated at the radar platform altitude. The phase screen was taken to be located halfway between the Earth's surface and the platform altitude. (Details of the propagation model are given in Appendix B.)

Figure 7 shows the signal-to-clutter ratio for the L-band system. The upper curve is for the two phase center implementation and the lower curve is for the three phase center implementation. As discussed in Section 2, DPCA performance, and consequently the signal-to-clutter ratio, is limited by numerous effects in addition to propagation effects. Since these effects are not explicitly included in the model, the DPCA improvement factor (shown in Figure 9) increases without bound as the decorrelation length increases. In reality, the DPCA improvement factor saturates at a finite value, typically on the order of 40 dB.

Figures 8, 9 and 10 demonstrate the behavior of the key elements that enter the signal-to-clutter calculation. As these results show, the performance degradation due to propagation effects results mainly from a combination of a loss of Doppler processing gain (Figure 8) and a degradation in DPCA clutter rejection (Figure 9). The DPCA target response (Figure 10) shows little degradation. The loss of Doppler processing gain is due to the combined effects of amplitude fading and phase scintillation. Amplitude fading can reduce the energy in the target signal and phase scintillation can spread the Doppler spectrum of a target return signal beyond the Doppler resolution of the radar; both show up as a reduction in Doppler processing gain. Losses due to DPCA clutter rejection occur from phase scintillation over the time separation Δ or spatial separation d of the two propagation paths. A phase imbalance of a fraction of a radian is sufficient to disrupt clutter rejection; hence, DPCA performance is disrupted when Δ is a small fraction of the signal decorrelation time or

(for the three phase center implementation) when d is a small fraction of the decorrelation length ℓ_0. Although severe scintillation can also cause a reduction in the signal-to-clutter ratio through antenna scattering loss, this effect becomes significant only at extremely small decorrelation lengths (at which Doppler processing losses and DPCA losses are severe).

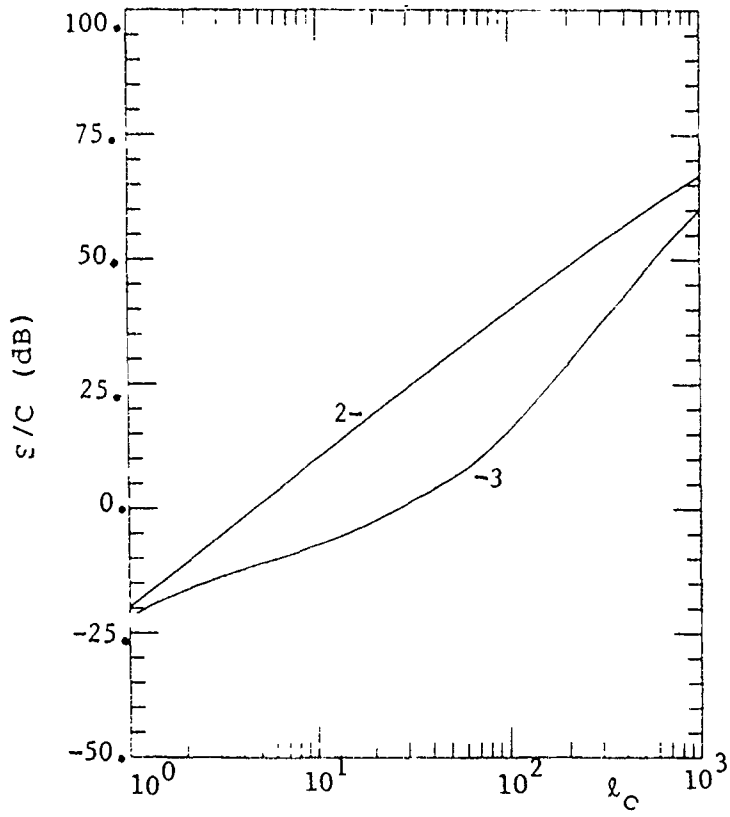

Figure 7. Signal-to-Clutter ratio as a function of decorrelation length for the parameters of Table 1: L-band.

As expected, the two phase center DPCA implementation is considerably more robust against propagation effects than the three phase center implementation. In fact, the two phase center implementation maintains a 15 dB signal-to-clutter ratio down to decorrelation lengths of 10 m, whereas the signal-to-clutter ratio for the three phase center implementation drops below 15 dB for decorrelation lengths less than 100 m.

A corresponding series of plots is shown for the UHF system in Figures 11–14. The same general trends are evident. Examination of these figures reveals that the candidate

UHF system could experience propagation-related performance disruptions due to naturally occurring ionospheric disturbances. In particular, for the parameters discussed in Appendix B for severe spread $F(\ell_0 \sim 250$ m), the two phase center system would have a signal-to-clutter ratio of 18 dB while a value of 0 dB would apply for the three phase center approach.

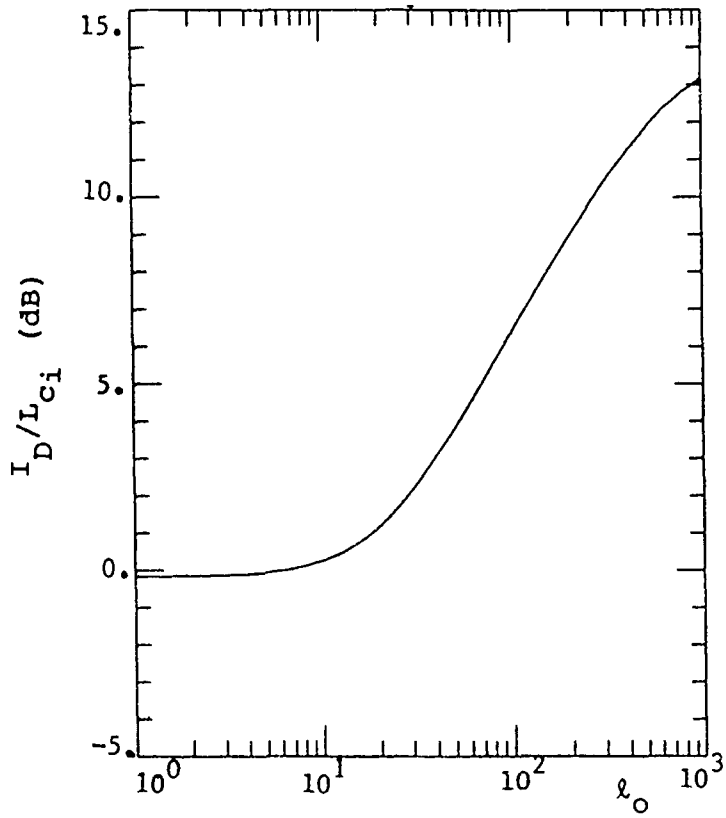

Figure 8. Doppler processing gain as a function of decorrelation length: L-band.

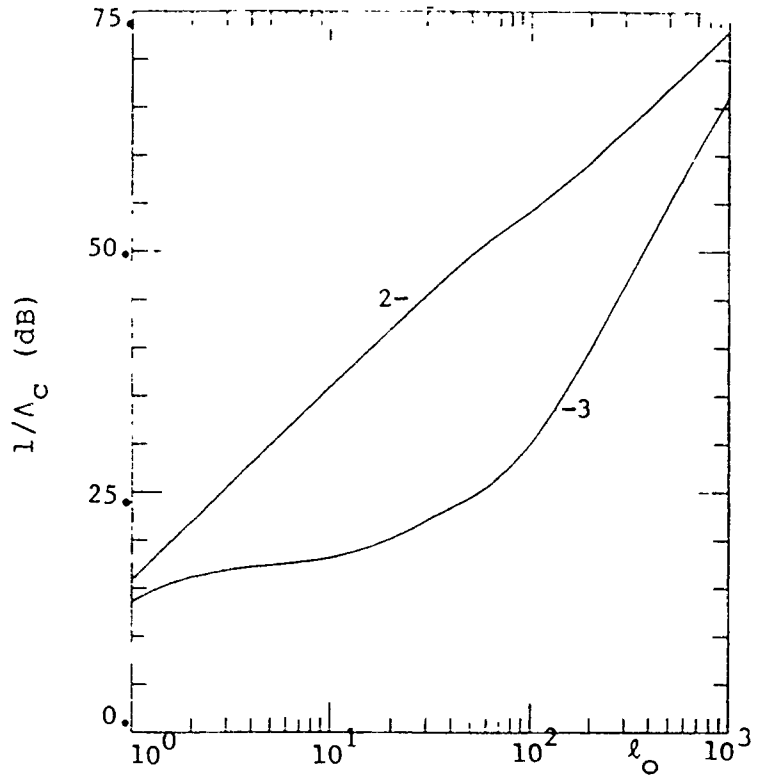

Figure 9. DPCA clutter rejection as a function of decorrelation length: L-band.

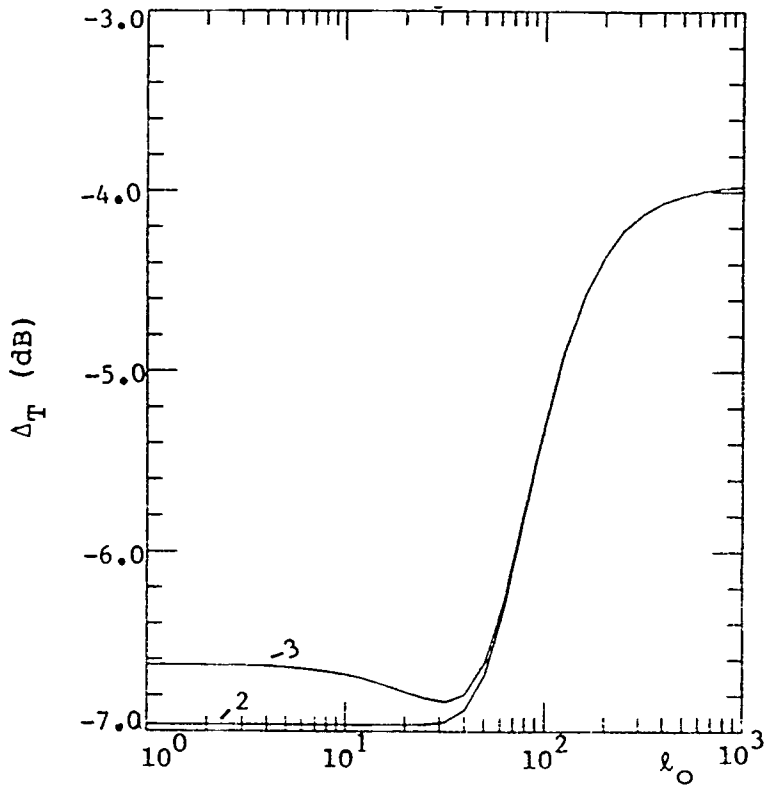

Figure 10. DPCA target response as a function of decorrelation length: L-band.

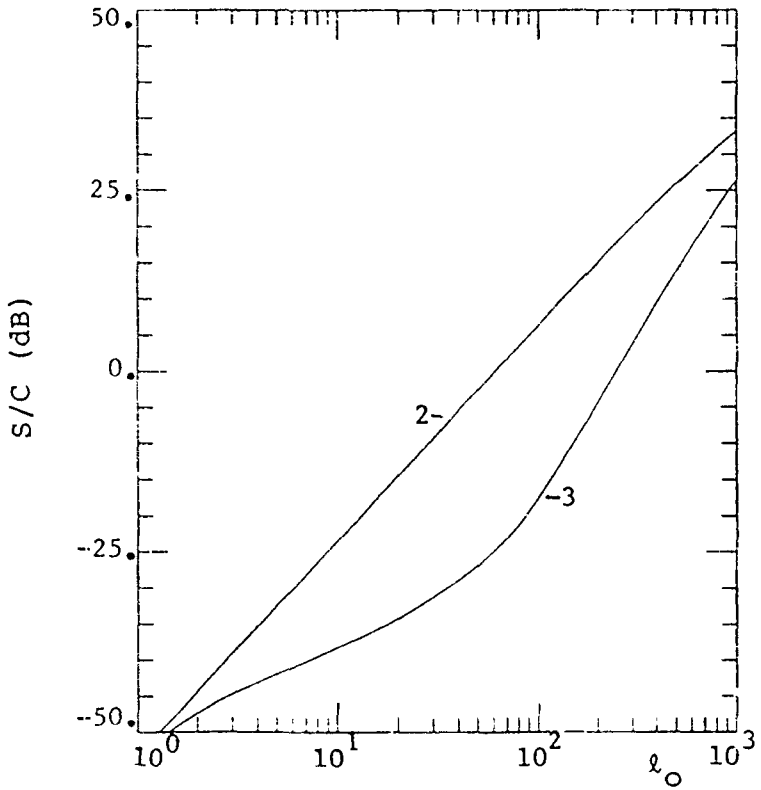

Figure 11. Signal-to-Clutter ratio as a function of decorrelation length for the parameters of Table 1: UHF.

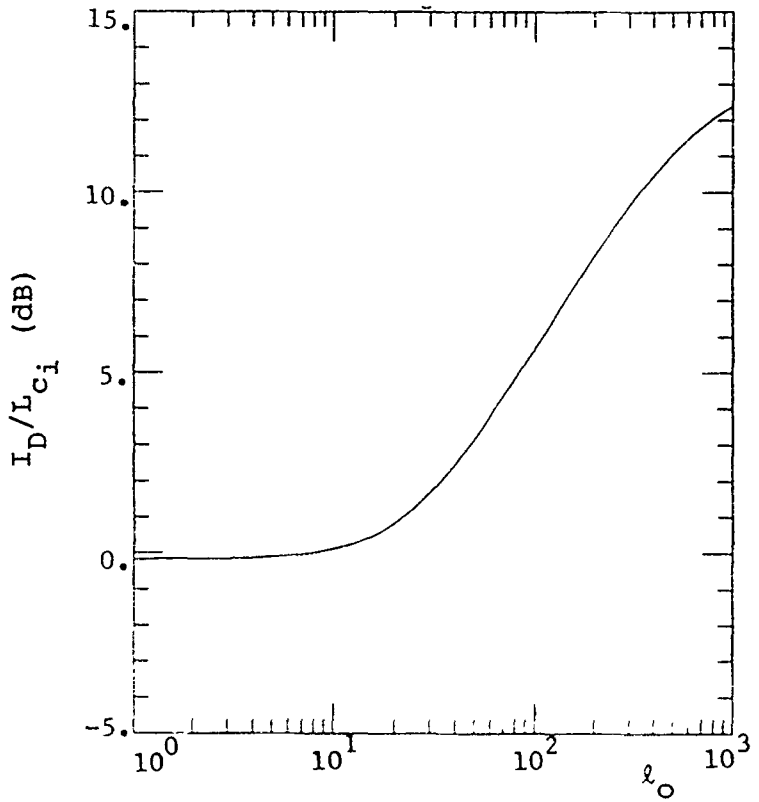

Figure 12. Doppler processing gain as a function of decorrelation length: UHF.

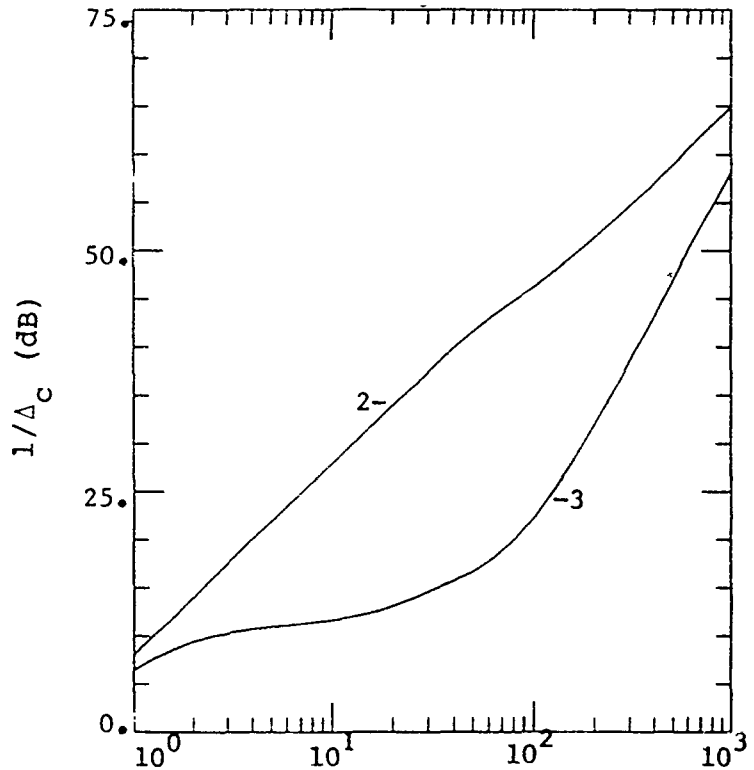

Figure 13. DPCA clutter rejection as a function of decorrelation length: UHF.

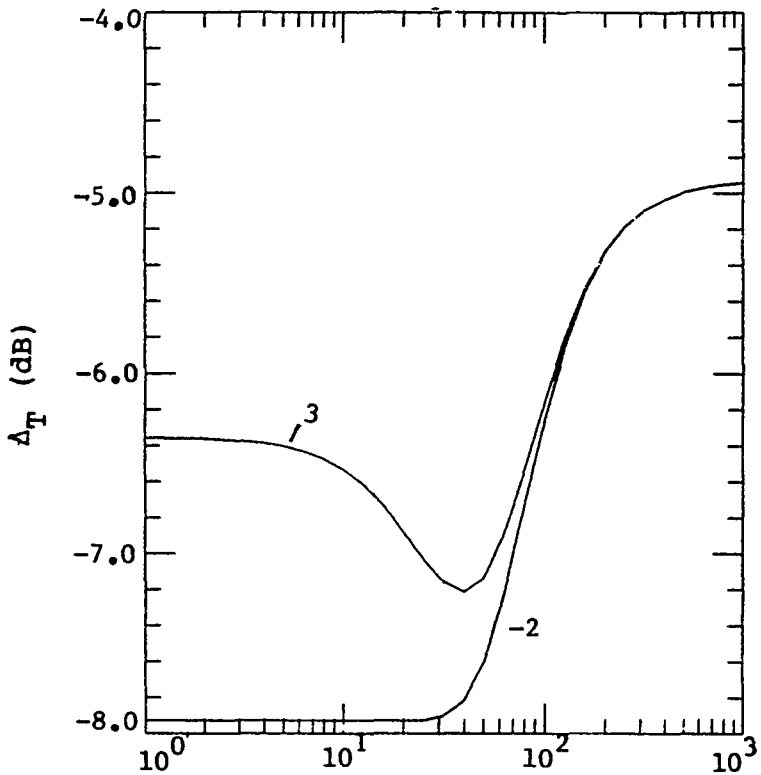

Figure 14. DPCA target response as a function of decorrelation length: UHF.

SECTION 4
CONCLUSIONS AND RECOMMENDATIONS FOR FURTHER WORK

A comprehensive model for the impact of ionospheric propagation effects on pulse-Doppler space-based radars in a target search mode has been developed. Propagation-induced DPCA degradation, Doppler processing losses, and antenna scattering losses are all properly incorporated. Our model differs from previous models of space-based radars with DPCA; previous models (Refs. 27–30) assumed that propagation effects had a negligible effect on DPCA cancellation. These previous studies quantified processing losses but did not quantify DPCA losses due to propagation effects. We find that DPCA processing losses can be significantly larger than Doppler processing losses.

Although the basic model is applicable to any degree of propagation disturbance, analytic results are possible only for Rayleigh scintillations. Phase screen simulations are necessary for less severe propagation environments for which non-Rayleigh statistics characterize the one-way path (Ref. 32).

Analytic results were presented for candidate L-band and UHF space-based radar under Rayleigh scintillating conditions ranging from relatively benign naturally occurring conditions to post-HANE conditions. All candidate systems were susceptible to considerable performance degradation in the post-HANE environment, although the two phase center L-band system was surprisingly robust. In all cases the two phase center implementation was considerably more robust than the three phase center implementation. The UHF system appears to be susceptible to performance degradation resulting from naturally occurring ionospheric conditions.

There are several obvious mitigants for propagation effects. The most obvious mitigant is the use of higher operating frequencies. Another mitigant is the use of a larger antenna aperture in the along-track direction. This narrows the Doppler spectrum of the clutter and produces less reliance on the very critical DPCA phase cancellation.

A lower platform altitude is another possible mitigant. This produces less difference in the DPCA path lengths and hence less disruption in the DPCA clutter cancellation. It may also be possible to avoid propagation through disturbed regions through use of sufficiently low platform altitudes.

The two phase center implementation is considerably more robust than the three phase center implementation. This is because although the two propagation paths are separated in time, they are over identical spatial paths. This implies that the two phase center implementation is susceptible only to the bulk striation drift.

There are numerous possibilities for additional work in this area. More detailed parameter studies, for example, the variation of signal-to-clutter ratio with target velocity for fixed values of decorrelation length, etc., can be performed. Phase screen simulations could be performed to more accurately characterize the onset of performance degradation. (As discussed above, the calculations performed in this manuscript were done under the assumption of Rayleigh scintillations.) In addition, it may be desirable to model additional radar modes such as a target tracking mode. (Calculations in this manuscript were performed for the degradation in signal-to-clutter ratio while in a target search mode.)

SECTION 5
LIST OF REFERENCES

1. Yeh, K. C., and Liu, C. H., "Radio Wave Scintillations in the Atmosphere" *Proc. IEEE*, Vol. 70, No. 4, April 1982, pp. 324–360.

2. Whitney, H. E., Aarons, J., Allen, R. S., and Seemann, D. R., "Estimation of the Cumulative Amplitude Probability Distribution Function of Ionospheric Scintillations," *Rad. Sci.* Vol. 7, pp. 1095–1104, 1972.

3. Pope, J. H., and Fritz, R. B., "High Latitude Scintillation Effects on Very High Frequency (VHF) and S-band Satellite Transmissions," *Indian J. Pure App. Phys.*, Vol. 9, pp. 593–600, August 1971.

4. Rino, C. L., Livingston, R. C., and Whitney, H. E., "Some New Results on the Statistics of Radio Wave Scintillation, 1. Empirical Evidence for Gaussian Statistics," *J. of Geo. Res.*, Vol. 81, No. 13, pp. 2051–2057, 1976.

5. Fremouw, E. J., Livingston, R. C., and Miller, D. A., "On the Statistics of Scintillating Signals," *J. Atmos. Terr. Phys.*, Vol. 42, pp. 717–731, 1980.

6. Taur, R. R., "Simultaneous 1.5- and 4-GHz Ionospheric Scintillation Measurements," *Rad. Sci.*, Vol. 11, pp. 1029–1036, December 1976.

7. Fremouw, E. J., Leadabrand, R. L., Livingston, R. C., Cousins, M. D., Rino, C. L., Fair, B. C., and Long, R. A., "Early Results from the DNA Wideband Satellite Experiment–Complex Signal Scintillation," *Rad. Sci.*, Vol. 13, No. 1, pp. 167–187, January–February, 1978.

8. Yeh, K. C. and Swanson, Jr., G. W., "The Scintillation of Radio Signals from Satellites," *J. Geophys. Res.*, Vol. 64, No. 12, pp. 2281–2286, 1959.

9. Skinner, N. J., Kellcher, R. F., Hacking, J. B., and Benson, C. W., "Scintillation Fading of Signals in the SHF Band," *Nature (Phys. Sci.)*, Vol. 232, pp. 19–21, 1971.

10. Davies, K., Fritz, R. B., Grubb, R N., and Jones, J. E., "Some Early Results from the ATS-6 Radio Beacon Experiment," *Radio Sci.*, Vol. 10, pp. 785–799, 1975.

11. Whitney, H. E., and Basu, S., "The Effect of Ionospheric Scintillation on VHF/UHF Satellite Communications," *Radio Sci.*, Vol. 12, pp. 123–133, 1977.

12. Johnson, A. L., and Lee, P. K., "Equatorial Scintillation Tests of LES 8/9," *Effect of the Ionosphere on Space and Terrestrial Systems*, Goodman, J. M., (ed.), pp. 25-30, U.S. Government Printing Office, 1978.

13. Mullen, J. P., Bushby, A., Lanat, J., and Pantoja, J., "Gigahertz Scintillation at the Magnetic Equator," *Effects of the Ionosphere on Space and Terrestrial Systems*, Goodman, J. M., (ed.), U.S. Government Printing Office, 1978.

14. Paulson, M. R., and Hopkins, R. U., "Spaced-Receiver Investigations of Equatorial Scintillation made at Guam during 1971 and 1976," *Effect of the Ionosphere on Space and Terrestrial Systems*, Goodman, J. M., (ed.), U.S. Government Printing Office, 1978.

15. Aarons, J., "Global Morphology of Ionospheric Scintillation," *Proc. IEEE*, Vol. 70, pp. 360–379, 1982.

16. Rino, C. L., "On the Application of Phase Screen Models to the Interpretation of Ionospheric Scintillation Data," *Rad. Sci.*, Vol. 17, No. 4, pp. 855–867, 1982.

17. Arendt, P. R., and Soicher, H., "Effects of Arctic Nuclear Explosions on Satellite Radio Communication," *Proc. EEE*, Vol. 52, No. 6, pp. 672–676, June 1964.

18. King, M. A., and Fleming, P. B., "An Overview of the Effects of Nuclear Weapons on Communications Capabilities," *Signal*, pp. 59–66, January 1980.

19. Matsushita, S., "On Artificial Geomagnetic and Ionospheric Storms Associated with High-Altitude Explosions," *J. Geophys. Res.*, Vol. 64, pp. 1149–1161, 1959.

20. Keyes, J. G., and Tinsley, B. A., "Optical Observations from Western Samoa of the Artificial Auroral Display, 9 July 1962.," *New Zealand J. Geol. Geophys.*, Vol. 5, pp. 925–932, 1962.

21. Rothwell, P., Wager, J. J., and Sayers, J., "Effect of the Johnston Island High-Altitude Nuclear Explosion on the Ionization Density in the Topside Ionosphere," *J. Geophys. Res.*, Vol. 68, pp. 947–949, 1963.

22. Maeda, H., Shirgaokar, A. J., Yashuhara, M., and Matsushita, S., "On the Geomagnetic Effect of the Starfish High-Altitude Nuclear Explosion," *J. Geophys. Res.*, Vol. 69, pp. 917–945, 1964.

23. Zinn, J., Hoerlin, H., and Petschek, A. G., "The Motion of Bomb Debris Following the Starfish Test," *Radiation Trapped in the Earth's Magnetic Field*, McCormac, B. M., (ed.), Dordrecht, The Netherlands: D. Reidel, pp. 671–692, 1966.

24. Boquist, W. P., and Snyder, J. W., "Conjugate Auroral Measurements from the 1962 U.S. High Altitude Nuclear Test Series," *Aurora and Airglow*, McCormac, B. M., (ed.), New York: Reinhold, pp. 325–339, 1967.

25. Hoerlin, H., *United States High-Altitude Test Experiences*, LA-6405, Los Alamos Scientific Laboratory, October 1976.

26. Glasstone, S., and Dolan, P. J., *The Effects of Nuclear Weapons*, 3rd ed., U.S. Department of Defense and the U.S. Department of Energy, 1977.

27. Dana, R. A., and Knepp, D. L., "The Impact of Strong Scintillation on Space Based Radar Design I: Coherent Detection," *Proc. IEEE*, Vol. AES-19, No. 4, pp. 539–549, 1983.

28. Knepp, D. L., and Dana, R. A., *The Impact of Strong Scintillation on Space Based Radar Design—Noncoherent Detection*, DNA-TR-83-43, MRC-R-788, Mission Research Corporation, November 1983.

29. Knepp, D. L., and Bradford, W. L., *Mitigation of Scintillation Effects on Space Based Radars Through Adoptive Non-coherent Processing*, DNA-TR-85-174, Mission Research Corporation, April 1985.

30. Knepp, D. L., and Dana, R. A., "The Impact of Strong Scintillation on Space Based Radar Design: Clutter Rejection," *Rad. Sci.*, Vol. 20, No.3, pp. 366–374, 1985.

31. Shrader, W. W., "MTI Radar," *Radar Handbook*, Skolnik, M. I., (ed.), McGraw Hill, pp. 17.9–17.11, 1970.

32. DeRaad, Jr., L. L., and Grover, M., *First-Order Intensity Statistics for Non-Rayleigh Fading*, DNA-TR-89-150, RDA-TR-0226128902-002, R & D Associates, February 1990.

33. Knepp, D. L., *Propagation of Wide Bandwidth Signals Through Strongly Turbulent Ionized Media*, Mission Research Corporation, DNA-TR-81-78, March 1982.

34. Knepp, D. L., *Multiple phase-Screen Propagation Analysis for Defense Satellite Communitions System*, DNA 4424T, MRC-R-33, Mission Research Corporation, September 1977.

35. Knepp, D. L., "Analytic Solution for the Two-Frequency Mutual Coherence Function for Sperhical Wave Propagation," *Rad. Sci.*, Vol. 18, No. 4, pp. 535-549, 1983.

36. Wittwer, L. A., *Radio Wave Propagation in Structured Ionization for Satellite Applications*, Defense Nuclear Agency, DNA-5304D, December 1979.

37. Knepp, D. L., and Wittwer, L. A., "Simulation of Wide Bandwidth Signals that have Propagated Through Random Media," *Rad. Sci.*, Vol. 19, No. 1, pp. 303-318, 1984.

38. Narcisi, R. S., and Szuszczewicz, E. P., "Direct Measurements of Electron Density, Temperature and Ion Composition in an Equatorial Spread-F Ionosphere," *J. Atm. Terr. Phys.*, Vol. 43, No. 516, pp. 463–471, 1981.

APPENDIX A
RADAR EQUATION DERIVATION

We will first give a few more details of the radar that enters the calculation of the radar equations. Each phase center of the radar has a (1-D) Gaussian aperture illumination function, $a(x)$, associated with it, appropriate to a side looking radar. Then, $a(x)$ is

$$a(x) = \frac{k_{0x}}{\sqrt{\pi}} \exp\left[-k_{0x}^2 x^2\right] \tag{A1}$$

where k_{0x} is related to the aperture size [see Eq. (A5)]. The one-way antenna radiation pattern as a function of ϵ, the angle from broadside, is then

$$G(\epsilon) = \left| \int_{-\infty}^{\infty} dx \; a(x) \exp(ik_0 x \sin\epsilon) \right|^2 = \exp\left[-\frac{k_0^2 \sin^2\epsilon}{2k_{0x}^2}\right] \tag{A2}$$

where $k_o(= 2\pi/\lambda)$ is th adar wave number. For small angles, $|\epsilon| \ll 1, G(\epsilon)$ can be approximated as

$$G(\epsilon) = \exp\left[-\frac{k_0^2 \epsilon^2}{2k_{0x}^2}\right]. \tag{A3}$$

If we require the 3 dB point to satisfy

$$G\left[|\epsilon| = \frac{1}{2}\frac{\lambda}{D}\right] = \frac{1}{2} \tag{A4}$$

where D is the azimuthal antenna length (called D_{az} in Section 2), then we have

$$k_{0x}^2 = \frac{\pi^2}{2\ell n 2 D^2}. \tag{A5}$$

The radar emits a coded pulse, which, upon matched filtering, produces a ground range resolution of δy. We will approximate the point spread function (PSF) as

$$PSF(y - y_0) = \begin{cases} 1, & |y - y_0| < \frac{1}{2}\delta y, \\ 0, & \text{otherwise}, \end{cases} \tag{A6}$$

Depending on the operating parameters of the radar, the range may or may not be ambiguous within the main lobe of the radar. If the range is ambiguous, contributions from all the ambiguous range cells must be included. The expressions for the signals that we will employ will always be after match filtering.

The background consists of a collection of scatterers, $A_j e^{i\phi} j$ located at positions x_j, y_j. We will assume the background is completely incoherent so that a simple model has ϕ_j a random variable uniformly distributed between 0 and 2π and A_j a constant, given by

$$A_j^2 = \sigma^0 / n_x n_y \tag{A7}$$

where $n_x(n_y)$ is the number of scatterers per unit length in the $x(y)$ direction.

In the following, we assume that the fading statistics are Rayleigh and separate the transfer function as follows [cf. Eq. (B6)]

$$h = h_s \exp[i\phi_1 + i\phi_2] \tag{A8}$$

where h_s represents the Rayleigh scintillation contribution and $\phi_1 + \phi_2$ is due to phase-only effects. As discussed in Appendix B, we divide the spectrum at a wave number K_R such that larger than K_R values contribute to the Rayleigh scintillation and smaller than K_R values contribute to the phase only effects. If we define the length, L_R, as

$$L_R = 2\pi / K_R, \tag{A9}$$

the phase-only effects are here further divided into two parts. The rationale for this division is that there is an additional scale of importance, L_S, the distance the radar travels during a dwell time. If $L_R < L_S$, we identify the contributions as

$$\phi_1 : \quad L_R < \text{scale size} < L_S,$$

$$\phi_2 : \quad L_S < \text{scale size}.$$

The ϕ_1 contribution will produce a Doppler spread since it leads to phase errors during the coherent integration time that are approximately averaged while ϕ_2 will lead to a Doppler shift since these phases, associated with long wavelengths, are essentially constant during the dwell time. If $L_S < L_R$, we only have ϕ_2 type contributions. This division of the spectrum is rather arbitrary but since the dominate effects are produced by the Rayleigh scintillations, the distinctions are not critical. In the following we assume the phase-only effects only affect the Doppler processing and are essentially constant for the DPCA operation [see Eq. (A26)].

The displaced phase center antenna is used to reject the signal due to stationary surface clutter. This is accomplished by making the phase center of the antenna electronically

adjustable as discussed in Section 2. Here, we will generalize the process, instead of restricting it to the two implementations discussed in Section 2. The operation consists of defining two series of pulses. The first series consists of pulses transmitted with the phase center at some location, designated X_1, as measured relative to the center of the physical antenna, and then received at phase center location Y_1. A second series is defined with the phase center located at X_2 for transmission and Y_2 for reception. These two series are essentially subtracted for surface clutter rejection. For this to happen, the location of the phase centers and the time separation of pulses have to be related, as discussed below.

The two phase center concept is defined by assuming

$$X_1 = Y_1 = d/2, \tag{A10a}$$

$$X_2 = Y_2 = -d/2. \tag{A10b}$$

It is to be noted that for a system deployed in space, the clutter, in general, will be moving due to the earth's rotation so the ray paths are not identical even for the clutter. As we will see, a slight altering of the processing that was discussed in Section 2 can reject the moving clutter and detect targets moving relative to the clutter. The three phase center concept is defined assuming

$$X_1 = X_2 = 0, \tag{A11a}$$

$$Y_1 = d/2, \tag{A11b}$$

$$Y_2 = -d/2. \tag{A11c}$$

It is clear for this implementation that the ray paths are not identical even for truly stationary clutter.

The starting point is the expressions for the returned signals for the two series. The coordinate system employed for the calculation is the rest frame of the disturbing medium. In addition we assume there is structure only in the along track direction ($x, \mathbf{i}$ = unit vector). If the center of the antenna is at $x = 0$, at $t = 0$, a point on the antenna (given by ξ or η relative to the phase center) for the first series of pulses is given by

$$r_1 = nTV + X_1 + \xi_1, \tag{A12a}$$

$$r_1 = (nT + t_d)V + X_1 + \eta_1. \tag{A12b}$$

Here, we have defined

$$
\begin{aligned}
n &= \text{pulse number,} \\
T &= \text{interpulse period for series 1 (or 2),} \\
r &= \text{position on transmit,} \\
u &= \text{position on receive,} \\
t_d &= 2R_o/c = \text{time delay,} \\
R_o &= \text{antenna} - \text{scatterer slant range,} \\
V &= \text{platform velocity.}
\end{aligned}
$$

For the second series, the corresponding positions are

$$
\begin{aligned}
r_2 &= (nT + \Delta)V + X_2 + \xi_1, \\
u_2 &= (nT + t_d + \Delta)V + Y_2 + \eta_1,
\end{aligned} \tag{A13}
$$

where Δ is the time separation between the two series. Note therefore that Δ is the time interval used for the DPCA processing and T is the time interval used for Doppler processing. The scatterers positions for the two series are given by

$$\mathbf{w}_1 = \mathbf{w}_o + nT\mathbf{v}, \tag{A14a}$$

$$\mathbf{w}_2 = \mathbf{w}_1 + \Delta\mathbf{v}, \tag{A14b}$$

where $\mathbf{w}_o$ is the initial position for the first pulse,

$$\mathbf{w}_0 = \mathbf{r}_T + \frac{1}{2}t_d\mathbf{v} \tag{A15}$$

and $\mathbf{v}$ is the velocity of the scatterer. In particular, if the scatterer is clutter, $\mathbf{v} = \mathbf{v}_E$, the earth's velocity in the rest frame of the media, and if it is a target, $\mathbf{v} = \mathbf{v}_E + \mathbf{v}_o$, where $\mathbf{v}_o$ is the velocity of the target relative to the earth. Under the usual conditions of a small radar footprint and a reasonably small dwell time, all slant ranges can be approximated as

$$\mathbf{R} = R_o + \Delta\mathbf{R}, \tag{A16a}$$

$$R = R_o + \mathbf{R}_o \cdot \Delta\mathbf{R}. \tag{A16b}$$

The returned signals for the two series after matched filtering are

$$s_1(n) = \sum_j A_j e^{i\phi_j} \int d\xi_1 \, d\eta_1 \; a(\xi_1)a(\eta_1)h(r_1, w_{1x})h(u_1, w_{1x}) \times \exp i\frac{2\pi}{\lambda}\left[2R_0 + \widehat{R}_0 \cdot (2nT\mathbf{v} - r_1\mathbf{i} - u_1\mathbf{i})\right], \tag{A17a}$$

$$s_2(n) = \sum_j A_j e^{i\phi_j} \int d\xi_1 \, d\eta_1 \; a(\xi_1)a(\eta_1)h(r_2, w_{2x})h(u_2, w_{2x}) \times \exp i\frac{2\pi}{\lambda}\left[2R_0 + \widehat{R}_0 \cdot (2nT\mathbf{v} + 2\Delta\mathbf{v} - r_2\mathbf{i} - u_2\mathbf{i})\right]. \tag{A17b}$$

Here, we have included point to point transfer functions from points on the antenna to points in the clutter or target. The integration over transmit and receive apertures will lead to finite aperture effects.

The DPCA processed signal is the appropriately weighted difference of s_1 and s_2,

$$T(n) = s_1(n) - e^{-i\beta}s_2(n). \tag{A18}$$

Noting that

$$r_2 + u_2 = r_1 + u_1 + 2\Delta V - (X_1 + Y_1 - X_2 - Y_2), \tag{A19}$$

we have

$$T(n) = \sum_j A_j e^{i\phi_j} \int d\xi_1 d\eta_1 \; a(\xi_1)a(\eta_1) \exp i\frac{2\pi}{\lambda}\left[2R_0 + \widehat{R}_0 \cdot (2nT\mathbf{v} - r_1\mathbf{i} - u_1\mathbf{i})\right] \times \left[h(r_1, w_{1x})h(u_1, w_{1x}) - e^{i\gamma}h(r_2, w_{2x})h(u_2, w_{2x})\right] \tag{A20}$$

where

$$\gamma = \frac{2\pi}{\lambda}\widehat{R}_0 \cdot \left[-2\Delta(V\mathbf{i} - \mathbf{v}) + (X_1 + Y_1 - X_2 - Y_2)\mathbf{i}\right] - \beta. \tag{A21}$$

Clearly, for the ambient environment, we must require γ to vanish for all scatterers that constitute the clutter. For a narrow beam with zero squint angle and look angle θ, $\widehat{R}_0$ for fixed range is approximately

$$\widehat{R}_0 = \mathbf{N} + \phi\mathbf{i} \tag{A22}$$

where $\mathbf{N}$ is the beam direction,

$$\mathbf{N} = (0, \sin\theta, -\cos\theta) \tag{A23}$$

and ϕ is the angle off beam center. The cancellation of the coefficient of ϕ determines Δ, the time separation of the two series,

$$\Delta = \frac{1}{2}\frac{X_1 + Y_1 - X_2 - Y_2}{V - v_{Ex}} \tag{A24}$$

while the part independent of ϕ determines β,

$$\beta = \frac{4\pi}{\lambda}\Delta \sin\theta v_{Ey}. \tag{A25}$$

With the proper choices of Δ and β, the DPCA processed signal can be written as

$$\begin{aligned} T(n) = \sum_j A_j e^{i\phi_{j_c}} e^{i\delta} e^{i\alpha} \exp i\frac{2\pi}{\lambda}\left[2R_0 + \hat{R}_0 \cdot \left(2nT(\mathbf{v}_E + \mathbf{v}_0 - V\mathbf{i}) - \mathbf{i}(t_d V + X_1 + Y_1)\right)\right] \\ \times \int d\xi_1 d\eta_1 \; a(\xi_1)a(\eta_1) \exp -i\frac{2\pi}{\lambda}\hat{R}_0 \cdot \mathbf{i}(\xi_1 + \eta_1) \\ \times \left[e^{-i\alpha} h_s(r_1, w_{1x}) h_s(u_1, w_{1x}) - e^{i\alpha} h_s(r_2, w_{2x}) h_s(u_2, w_{2x})\right] \end{aligned} \tag{A26}$$

where, again, $\mathbf{v}_0$ is the velocity of the target relative to the earth. The phase only effects are contained in δ,

$$\delta = 2\phi_2(nTV, x_j) + \phi_1(nTV, x_j) + \phi_s\left((nT + t_d)V, x_j\right), \tag{A27)}$$

which refers to both the antenna position, for example, nTV, and the location of the scatterer, x_j, and makes use of the fact that these effects are associated with long wavelengths. We have also defined α as

$$\alpha = \begin{cases} 0, & \text{clutter}, \\ \frac{2\pi}{\lambda}\Delta\hat{R}_0 \cdot \mathbf{v}_0, & \text{target}. \end{cases} \tag{A28}$$

The DPCA signal is Doppler processed to detect moving targets. For the purposes of analysis, we will employ a simple, unweighted, Doppler filter, given by

$$D(V_D) = \frac{1}{N}\sum_{n=0}^{N-1} e^{+i\frac{4\pi}{\lambda}TV_D n} T(n), \tag{A29a}$$

$$|V_D| < \frac{1}{2}\frac{\lambda}{2T}, \tag{A29b}$$

where N is the total number of pulses in the coherent integration time. In particular, the quantity we will investigate is the average value of the square,

$$\left\langle \left|D(V_D)\right|^2 \right\rangle = \frac{1}{N^2}\sum_{n,n'=0}^{N-1} e^{+i\frac{4\pi}{\lambda}TV_D(n-n')} < T(n)T^*(n') > . \tag{A30}$$

We note here that since the background is modeled as a set of incoherent scatterers, we have the effective replacement

$$\sum_j \sum_{j} A_j A_j' e^{i\phi j} e^{-i\phi j'} \rightarrow \frac{\sigma^0 \delta y}{n_x} \sum_{x_j}' \ldots \tag{A31}$$

where x_j is a sum over an azimuthal line of scatterers. As for the target, we have

$$A_T A_T^* \ldots \rightarrow \sigma \ldots . \tag{A32}$$

For the phase only effects, we have

$$< e^{i\delta} e^{-i\delta'} >= e^{2i\left[\phi_2(nTV,x_j)-\phi_2(n'TV,x_j)\right]} e^{-\Gamma} \tag{A33}$$

where

$$\begin{aligned} \Gamma = {} & 2C_1(0) + 2C_1(t_d V) - 2C_1\left[(n-n')TV\right] \\ & - C_1\left[(n-n')TV + t_d V\right] - C_1\left[(n-n')TV - t_d V\right]. \end{aligned} \tag{A34}$$

Here, $C_1(x)$ is the phase correlation function that arises from that part of the spectrum that contributes to ϕ_1.

The Rayleigh scintillation contribution can be readily calculated using Eqs. (B9) and (B10). In addition, with the assumed aperture illumination function, Eq. (A1), the aperture integrals are straightforward. The fact that ϕ_2 depends on the scatterer location can complicate the sum over the background scatterers. However, it is known that Doppler processing essentially selects a restricted region of the footprint such that the scatterers have the appropriate Doppler shift. Since ϕ_2 is assumed to vary slowly, we can treat x_j in Eq. (A33) as effectively constant. However, since the target and the clutter it is competing against in a given Doppler cell are physically located at different azimuth positions, the Doppler shifts arising from ϕ_2 will be different. (Typical magnitudes of these shifts will be discussed in Appendix B.) Therefore, for the clutter contribution, the sum over the

background scatterers can be effectively approximated by a Gaussian integral. We then find

$$\langle T(n)T^*(n')\rangle_{\text{clutter}} = \sigma_c \frac{1}{\sqrt{S}} \langle e^{i\delta} e^{-i\delta'} \rangle e^{-i\frac{4\pi}{\lambda} T\mathbf{N}\cdot\mathbf{W}(n-n')}$$
$$\times \exp -\left[k_{0x}^2 S(\mathbf{i}\cdot\mathbf{W})^2 + \frac{2}{S\ell_0^2} V_1^2 \right] T^2 (n-n')^2$$
$$\times \left\{ A - 2B \exp -k_{0x}^2 S \left(\frac{S-1}{S} \right)^2 \Delta^2 V_2^2 \cosh \left[\frac{4\Delta}{\ell_0^2} T V_2^2 (n-n') \right] \right\}, \tag{A35}$$

$$\langle T(n)T^*(n')\rangle_{\text{Target}} = \sigma \frac{1}{S} \exp -\frac{4\pi^2}{k_{0x}^2 \lambda^2} \frac{1}{S} (\hat{R}_0 \cdot \mathbf{i})^2 \langle e^{i\delta} e^{-i\delta'} \rangle$$
$$\times e^{-i\frac{4\pi}{\lambda} T\hat{R}_0\cdot(\mathbf{W}-\mathbf{v}_0')(n-n')} \exp -\frac{2}{S\ell_0^2} V_1^2 T^2 (n-n')^2$$
$$\times \left\{ A - Be^{2i\tilde{\alpha}} \exp -\frac{4\Delta}{S\ell_0^2} V_1 V_2 T(n-n') \right.$$
$$\left. - Be^{-2i\tilde{\alpha}} \exp \frac{4\Delta}{S\ell_0^2} V_1 V_2 T(n-n') \right\} \tag{A36}$$

where (identified as S_{az} in Section 2)

$$S = 1 + \frac{2}{\ell_0^2 k_{0x}^2} = 1 + \frac{4\ell n 2}{\pi^2} \frac{D^2}{\ell_0^2}. \tag{A37}$$

We note the bounds

$$0 \le \frac{1}{S\ell_0^2} < \frac{\pi^2}{4\ell n 2} \frac{1}{D^2}, \tag{A38a}$$

$$0 \le \frac{2}{k_{0x}^2 \ell_0^2 S} \le 1. \tag{A38b}$$

The effective velocity of the clutter in the center of the beam is $\mathbf{W}$,

$$\mathbf{W} = V\mathbf{i} - \mathbf{v}_E - \frac{S-1}{S}\mathbf{i}\left[V + \frac{R_+}{R_-} v_{Ex} \right] \tag{A39}$$

while the effective target velocity relative to $\mathbf{W}$ is

$$\mathbf{v}_0' = \mathbf{v}_0 + \frac{S-1}{S} \frac{R_+}{R_-} v_{0x}\mathbf{i}. \tag{A40}$$

For DPCA, the target velocity has been effectively changed such that [cf. Eq. (A28)]

$$\tilde{\alpha} = \frac{2\pi}{\lambda} \Delta\hat{R}_0 \cdot \left(\mathbf{v}_0 + \frac{S-1}{S} \left(v_{Ex} + \frac{R_+}{R_-} v_{Ex} + \frac{R_+}{R_-} v_{0x} \right) \mathbf{i} \right). \tag{A41}$$

We have also defined various velocities as

$$V_1 = V + \frac{R_+}{R_-} v_x, \tag{A42}$$

$$V_2 = v_{Ex} + \frac{R_+}{R_-} v_x. \tag{A43}$$

The clutter contribution is proportional to the total clutter cross section for a range cell, σ_c,

$$\sigma_c = \frac{1}{2\sqrt{\pi}} \sigma^0 \delta y R_0 \lambda k_{0x}. \tag{A44}$$

The coefficients A and B are given as

$$A = 2 + \exp -2(X_1 - Y_1 - t_d V)^2 / S\ell_0^2 + \exp -2(X_2 - Y_2 - t_d V)^2 / S\ell_0^2, \tag{A45}$$

$$\begin{aligned} B = \exp\left[-\frac{2\Delta^2}{S\ell_0^2} V_2^2\right] \Bigg\{ & \exp -\frac{1}{S\ell_0^2}\left[(X_1 - X_2)^2 + (Y_1 - Y_2)^2 - \frac{1}{2}(X_1 + Y_1 - X_2 - Y_2)^2\right] \\ & + \exp -\frac{1}{S\ell_0^2}\Bigg[(Y_1 - X_2)^2 + (X_1 - Y_2)^2 - \frac{1}{2}(X_1 + Y_1 - X_2 - Y_2)^2 \\ & + 2t_d V(Y_1 + Y_2 - X_1 - X_2) + 2(t_d V)^2\Bigg]\Bigg\}. \end{aligned} \tag{A46}$$

The particular expressions for the two and three phase center concepts discussed in Section 2 are, for the two phase center concept,

$$A_2 = 2(1 + \exp -2(t_d V)^2 / S\ell_0^2), \tag{A47a}$$

$$B_2 = \frac{1}{2} A_2 \exp -\frac{2\Delta^2}{S\ell_0^2} V_2^2, \tag{A47b}$$

and, for the three phase center concept,

$$A_3 = 2 + \exp -2\left(t_d V + \frac{d}{2}\right)^2 / S\ell_0^2 + \exp -2\left(t_d V - \frac{d}{2}\right)^2 / S\ell_0^2, \tag{A48a}$$

$$B_3 = \exp -\frac{2\Delta^2}{S\ell_0^2} V_2^2 (\exp -d^2/2S\ell_0^2 + \exp -2(t_d V)^2 / S\ell_0^2). \tag{A48b}$$

Note that we have for the two implementations [cf. Eq. (A24)]

$$\begin{aligned} \text{two:} \quad & \Delta = d/(V - v_{Ex}), \\ \text{three:} \quad & \Delta = \tfrac{1}{2} d/(V - v_{Ex}), \end{aligned} \tag{A49}$$

while convenient, but not necessary, choices for T are

$$\begin{aligned} \text{two:} \quad & T = 2\Delta, \\ \text{three:} \quad & T = \Delta. \end{aligned} \tag{A50}$$

For the Doppler processing, we will approximate the phase only effects as [cf. Eq. (A33)]

$$\phi_2(nTV, x_j) - \phi_2(n'TV, x_j) = C_2(x_j)(n - n'), \tag{A51a}$$

$$\Gamma = C_1(n - n')^2, \tag{A51b}$$

(see Appendix B). We also notice that the $(n - n')$ dependence inside the $\{\ \}$ in Eq. (A35) and Eq. (A36) have small coefficients and, to first approximation, can be ignored. This allows the ionospheric effects on DPCA and Doppler to be separated. The Doppler processing for both the target and clutter then have the general form

$$\begin{aligned} F(\xi, Z) &= \frac{1}{N^2} \sum_{n,n'=0}^{N-1} e^{i2\pi\zeta(n-n')} e^{-Z(n-n')^2} \\ &= \frac{1}{N} \sum_{n=-(N-1)}^{N-1} \left(1 - \frac{|n|}{N}\right) e^{2\pi i\xi n} e^{-Zn^2} \end{aligned} \tag{A52}$$

where

$$|\xi| \leq \frac{1}{2}. \tag{A53}$$

The expressions for ξ and Z for the clutter and target can be determined from Eqs. (A35) and (A36), respectively, and Eq. (A30).

The maximum response of the Doppler processed target signal is characterized by

$$F(\xi = 0, Z_T) \sim \left[1 + \frac{2}{\pi} N \sqrt{\frac{Z_T}{\pi}} + N^2 \frac{Z_T}{\pi}\right]^{-\frac{1}{2}}, \tag{A54}$$

$$Z_T = \frac{2}{S\ell_0^2} V_1^2 T^2 + C_1. \tag{A55}$$

The requirement of $\xi = 0$ determines a particular Doppler velocity, V_D, the Doppler bin with peak response, that satisfies

$$V_D = \widehat{R}_0 \cdot (\mathbf{W} - \mathbf{v}_o') - \frac{C_2(T)}{\pi} \frac{\lambda}{2T} + \frac{\lambda}{2T} \ell \tag{A56}$$

where ℓ is an integer (the Doppler velocity may be ambiguous) such that Eq. (A29b) is satisfied and $C_1(T)$ is the appropriate value for the target location in the footprint.

The clutter processed signal at Doppler velocity V_D is characterized by

$$F(\xi, Z_c) \sim \sqrt{\frac{\pi}{Z_c N^2}} \exp -\pi^2 \xi^2 / Z_c \tag{A57}$$

where

$$Z_c = k_{ox}^2 S(\mathbf{i}\cdot\mathbf{W})^2 T^2 + \frac{2}{S\ell_0^2} V_1^2 T^2 + C_1 \tag{A58a}$$

$$\sim k_{ox}^2 (V - v_{ex})^2 T^2 \tag{A58b}$$

and

$$\xi = \frac{1}{\lambda/2T}\left[(\widehat{R}_o - \mathbf{N})\cdot\mathbf{W} - \widehat{R}_o\cdot\mathbf{v}_o'\right] + \ell' + \frac{C_2(C) - C_2(T)}{\pi} \tag{A59}$$

where ℓ' is an integer such that Eq. (A53) is satisfied and $C_2(C)$ is the appropriate value for the interfering clutter.

The above simplifications, including the separation of DPCA and Doppler effects, lead to the following simple approximate expression for the signal to clutter ratio,

$$S/C = \frac{\sigma}{\sigma_c}\frac{I_{DPCA} I_D I_A}{S^{\frac{1}{2}} L_B L_{ci}}. \tag{A60}$$

In the above, we have

$$\sigma = \text{average target cross section}$$

$$\sigma_c = \text{average surface clutter cross section}$$

$$= \frac{1}{2}\left[\frac{\pi}{2\ell n 2}\right]^{\frac{1}{2}} \sigma^0 \delta y \frac{\lambda R_0}{D} n \tag{A61}$$

$$n = \text{number of ambiguous range cells}$$

$$I_{\text{DPCA}} = \text{DPCA improvement factor}$$

$$= \Delta_T/\Delta_C \tag{A62}$$

$$I_D = \text{Doppler improvement factor for clutter}$$

$$= \left[\frac{\pi}{2\ell n 2}\right]^{\frac{1}{2}} \frac{VT_c}{D} \tag{A63}$$

$$I_A = \text{antenna pattern improvement factor}$$

$$= \exp 8\ell n 2 \frac{D^2 v_t^2}{\lambda^2 V^2} \tag{A64}$$

$$L_B = \text{beam loss due to target location}(\widehat{R}_o)$$

$$= \exp 8\ell n 2 \frac{D^2}{\lambda^2}\frac{1}{S}(\widehat{R}_o\cdot\mathbf{i}) \tag{A65}$$

$$L_{ci} = \text{coherent integration loss for target Doppler}$$

$$= \left[1 + \frac{2}{\pi} N \sqrt{\frac{Z_T}{\pi}} + N^2 \frac{Z_T}{\pi}\right]^{\frac{1}{2}}. \tag{A66}$$

For DPCA, the difference signals for target (T) and clutter (C) are

$$\Delta_T = A - 2B\cos 2\bar{\alpha}, \tag{A67a}$$

$$\Delta_C = A - 2B\exp -\frac{\pi^2}{2\ell n2} S\left[\frac{S-1}{S}\right]^2 (V_2\Delta/D)^2. \tag{A67b}$$

The results for the two candidate systems discussed in Section 3 were calculated using Eq. (A60). To indicate the adequacy of this approximation, we can define correction factors for the target (T) and clutter (C) as

$$\text{corr } (T) = \frac{SL_BL_{ci}}{\sigma\Delta_T}\langle|D_T|^2\rangle, \tag{A68a}$$

$$\text{corr } (C) = \frac{\sqrt{S}I_DI_A}{\sigma_c\Delta_C}\langle|D_C|^2\rangle. \tag{A68b}$$

The correction factors are the ratios of the exact results, Eq. (A30), for target [Eq. (A36)] and clutter [Eq. (A35)], and the approximate expressions leading to Eq. (A60).

For the parameters discussed in Section 3, the correction factors as a function of ℓ_o are shown in Figure 15. It can be seen that the correction factors are essentially unity except for small decorrelation lengths at L-band where they tend to further degrade performance.

The form of the antenna improvement factor, Eq. (A64), employed in Eq. (A60) is based on the simple estimate of Eq. (A57). This is adequate if ξ is sufficiently close to zero but can be seriously in error over part of the Doppler spectrum. As illustrations of this effect, Figure 16 shows the antenna improvement factor as predicted by Eq. (A52) and as given by Eq. (A64) for the three phase center implementation of the two systems discussed in Section 3. It is clear that both systems deviate significantly from the simple expression, Eq. (A64). Note that $\xi = 0.072$ for the L-band system and $\xi = 0.064$ for the UHF system. The clutter errors, Figure 15, for large values of ℓ_o are due to the inaccurate calculation of the antenna improvement factor. The first error was that Eq. (A64) was used with $V \to V - v_{ex}$ [cf. Eqs. (A57) and (A58b)] leading to overestimates of 1.4 dB at L-band and 0.25 dB at UHF. In addition, Figure 16 implies an additional 0.6 dB error at L-band and about -0.1 dB at UHF. The total errors are approximately 2 dB at L-band and 0.15 dB at UHF.

Finally, it should be noted that the form of Eq. (A60) ignores the Doppler shifts induced by the phase only contribution to the ionospheric transfer function. As discussed in Appendix B, this shift can be significant. The actual antenna improvement factor that should

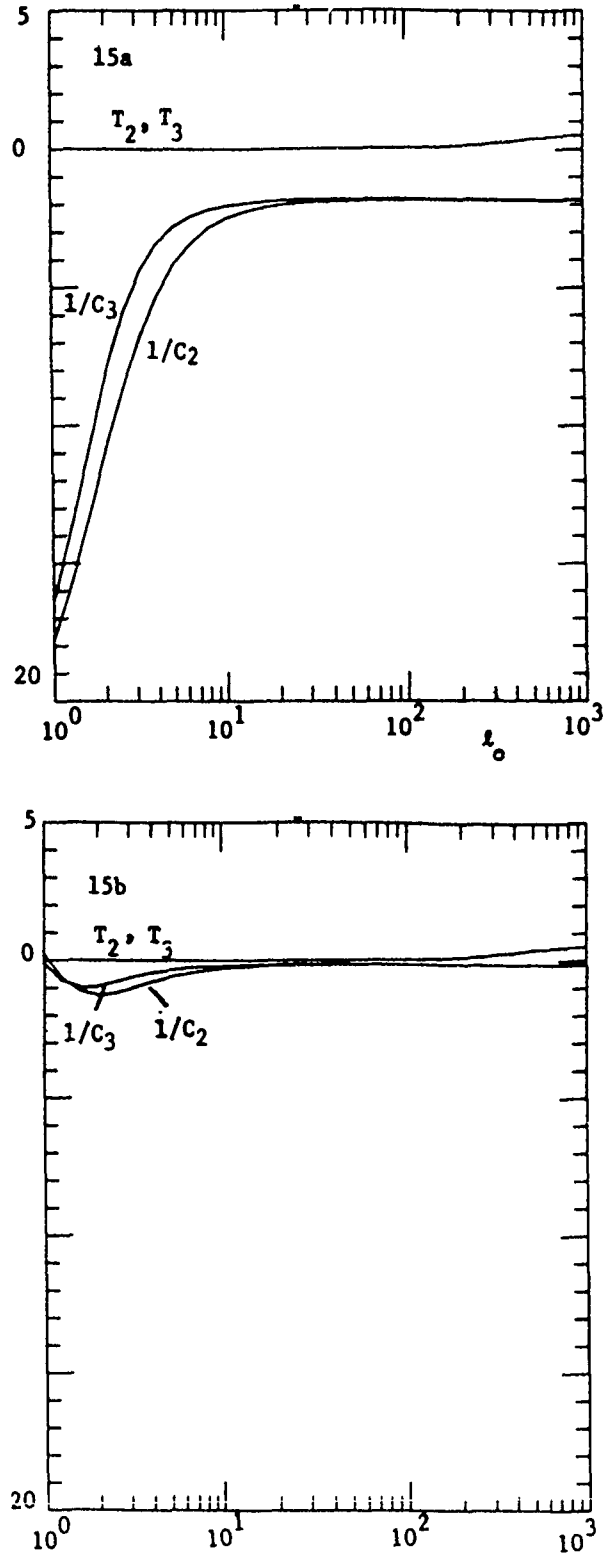

Figure 15. Correction factors for target (T) and clutter (C) versus ℓ_0: (a) L-band, (b) UHF.

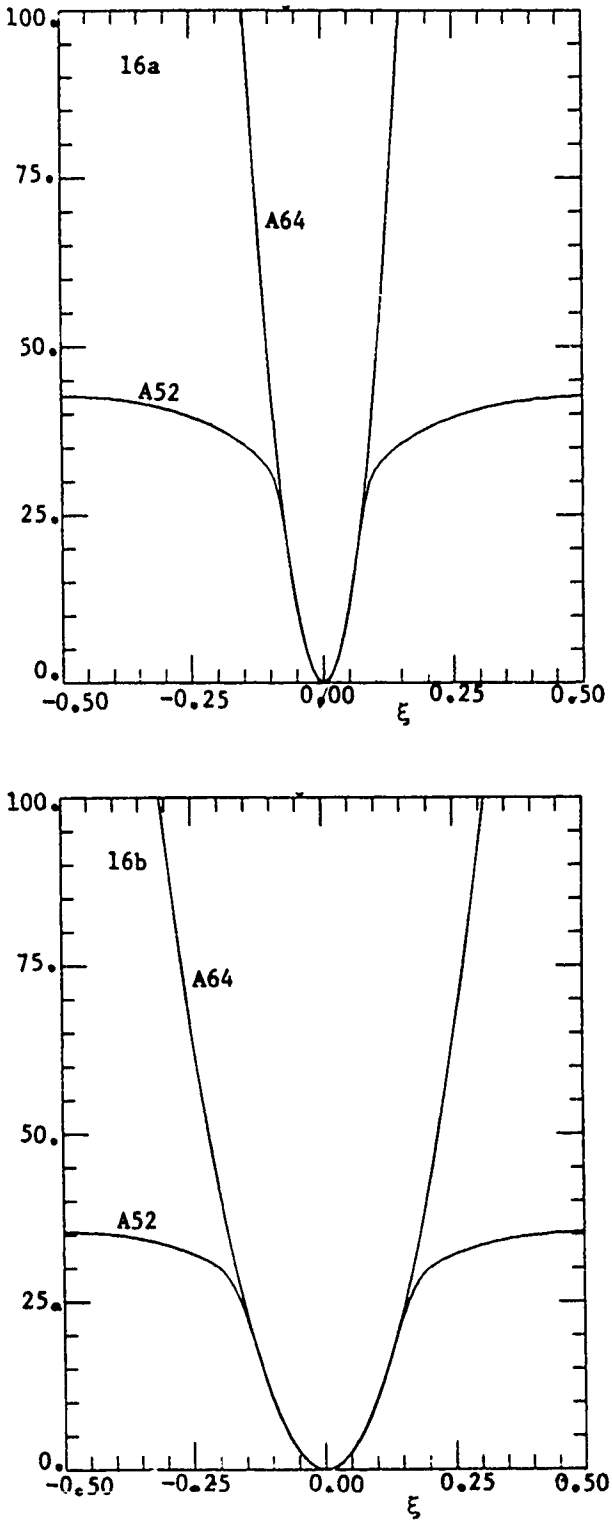

Figure 16. Antenna pattern improvement factor as calculated by simple estimate [Eq. (A64)] and exactlty [Eq. (A52)]; a) L-band, b) UHF.

be used in Eq. (A60) should be evaluated at the value of ξ given in Eq. (A59). Since the term arising from C_2 is a Gaussian random variable, the target can easily be shifted such that the interfering clutter increases and the antenna improvement factor decreases.

APPENDIX B
CHARACTERIZATION OF THE ENVIRONMENT

The presence of an electron density influences the propagation of an electromagnetic wave by introducing an additional (over vacuum) differential phase change per unit length of the propagation path, ℓ, given by

$$\frac{d\phi}{d\ell} = r_e \lambda n_e(\mathbf{r}, t) \tag{B1}$$

where ϕ is the phase, r_e is the classical radius of the electron ($r_e = 2.82 \times 10^{-15}$ m) and n_e is the local electron number density. This assumes that the electron density is not so high that absorption dominates. The total electron density can be partitioned into an average value, $< n_e >$, and a fluctuating contribution, $\delta n_e(\mathbf{r}, t)$, as

$$n_e(\mathbf{r}, t) = < n_e > + \delta n_e(\mathbf{r}, t). \tag{B2}$$

The average value leads to total electron content (TEC) effects and as can be seen from Eq. B1, will be frequency dependent. For a generic radar system, the TEC effects would affect ranging since the coded pulse has some finite bandwidth B. The effects include spreading the range resolution cell and introducing phase errors for the signal contribution of individual scatterers. However, the systems of interest have reasonably small bandwidths (megahertz) and moderately high frequencies (VHF and above) so that these effects only become important for severe environments where other effects have already significantly degraded performance. For this report, we will not consider frequency effects within the bandwidth of the radar.

The effects of the fluctuating part can be viewed as follows (Refs. 33–34). Consider an electromagnetic wave incident on an extended region of disturbed electron density such as the ionosphere. Initially, the wave experiences phase changes that are random from one location to another. These random phase fluctuations produce distortions in the wave front which in turn leads to diffraction. As the perturbed wave propagates into the disturbed region, it can break up into additional ray paths that can further diffract and scatter. Consequently, if we consider a point source on one side of a perturbed region and some point (scatterer) on the other, the electromagnetic field that reaches the point may have propagated along a number of more or less independent paths. The total field present, being a coherent sum of the contributions from different paths, can have significant differences in phase and amplitude from that given by free space propagation. We can define a transfer

function, h, from a source on one side of the perturbing media ($\mathbf{r}_+$) to a point on the other side ($\mathbf{r}_-$) as the ratio of the actual electric field present (E) to the free space electric field (E_o),

$$h(\mathbf{r}_+, \mathbf{r}_-, t) = E(\mathbf{r}_+, \mathbf{r}_-, t)/E_o(\mathbf{r}_+, \mathbf{r}_-). \tag{B3}$$

Here, the time t refers to changes in the media which occur on scales much slower than the time scale set by the bandwidth of the radar, $1/B$.

The actual characterization of the medium, $n_e(\mathbf{r}, t)$, is never known. Instead, the medium is described in statistical terms. Likewise, the solution to the transfer function is not available so it is also described statistically. The second order statistics are determined by the mutual coherence function, Γ_1, defined as

$$\Gamma_1(\mathbf{r}_{1+}, \mathbf{r}_{1-}, \mathbf{r}_{2+}, \mathbf{r}_{2-}, t_1, t_2) = \left\langle h(\mathbf{r}_{1+}, \mathbf{r}_{1-}, t_1) h^*(\mathbf{r}_{2+}, \mathbf{r}_{2-}, t_2) \right\rangle. \tag{B4}$$

This is the primary quantity of interest in the study of communication channels. However, since radar employs two way paths through the media, the primary quantity of interest is the fourth order statistics, given, in an obvious notation, by

$$\Gamma_2(1,2,3,4) = \left\langle h(1)h(2)h^*(3)h^*(4) \right\rangle. \tag{B5}$$

Approximate analytic solutions are available for Γ_1 in terms of the statistics of $\delta n_e(\mathbf{r}, t)$ (Ref. 35). A general result for Γ_2 is not available. However, it has been determined that under strong scattering conditions (Refs. 36, 37) the channel transfer function can be usefully partitioned as

$$h = h_s \exp[i\phi_L], \tag{B6}$$

where ϕ_L is a Gaussian process and the real and imaginary parts of h_s are zero-mean, equal variance, uncorrelated Gaussian random variables.

In this formulation, the total, sight-path-integrated phase (i.e., from Eq. B1) is also partitioned as $\phi = \phi_s + \phi_L$. This is done in such a manner (Ref. 37) that ϕ_L is spatially slowly varying and therefore does not cause significant scattering and multipath effects. Then Γ_1 can also be partitioned, at least heuristically, as

$$\Gamma_1(1,2) = \Gamma_{1s}(1,2) \exp\left[i(\phi_L(1) - \phi_L(2))\right], \tag{B7}$$

where Γ_{1s} is the mutual coherence function arising from effects caused by ϕ_s. In the thin phase screen approximation, Γ_{1s} is given as

$$\Gamma_{1s}(1,2) = \exp\left(C_{\phi_s}(1,2) - \sigma^2_{\phi_s}\right), \tag{B8}$$

where $\sigma^2_{\phi_s}$ is the variance, and $C_{\phi_s}(1,2)$ the covariance, of ϕ_s.

Most important for present purposes is the conclusion that, since h_s may now be regarded as a complex Gaussian process, with additional properties as cited above, under these strong scattering conditions h_s is fully defined by its second order statistics, or Γ_{1s}. The needed relationship for Γ_2 can then be given as

$$\Gamma_2(1,2,3,4) = \left\langle \exp i\big(\phi_L(1) + \phi_L(2) - \phi_L(3) - \phi_L(4)\big)\right\rangle \times \left[\Gamma_{1s}(1,3)\Gamma_{1s}(2,4) + \Gamma_{1s}(1,4)\Gamma_{1s}(2,3)\right]. \tag{B9}$$

A further simplification will be obtained from the assumption that the scattering ionospheric medium evolves on short-to-intermediate time scales (i.e., seconds-to-minutes) primarily through an overall uniform drift relative to the radar sight path(s). With this so-called "Taylor frozen-in" hypothesis, the medium will be assumed to be time independent in its rest frame, which is the coordinate system employed for the calculations of Appendix A. In addition, Γ_{1s}, Eq. B8, will be approximated by assuming (a) structure occurs only in the along-track direction, (b) the two sides of the perturbing media are related by the thin phase screen result, and (c) an effective decorrelation length at the radar platform, ℓ_0, is introduced. The particular expression we will employ is

$$\Gamma_{1s}(1,2) = \exp -(X_1 - X_2)^2/\ell_0^2 \tag{B10}$$

where

$$X = x_+ + \frac{R_+}{R_-}x_-. \tag{B11}$$

Here, x_+ refers to the radar side of the perturbing media, x_- to the clutter and target side and $R_+(R_-)$ is the distance from the center of the perturbing media to the radar (clutter). We now turn to a discussion of the relationship between ℓ_0 and the perturbing media.

The electron power spectral density (PSD) is defined as

$$\left\langle \delta n_e(\mathbf{r})\delta n_e(\mathbf{r}')\right\rangle = \int \frac{d\mathbf{K}}{(2\pi)^3}\Phi_{\delta n}(\mathbf{K})e^{i\mathbf{K}\cdot(\mathbf{r}-\mathbf{r}')}. \tag{B12}$$

Experimental evidence suggests that a reasonable PSD has a power law behavior of K^{-4} for large K and is symmetric around the ambient magnetic field direction. If we assume a

K^{-n} behavior, a convenient power law PSD is (Ref. 33)

$$\Phi_{\delta n}(\mathbf{K}) = \sigma_{Ne}^2 (2\pi\beta)^{\frac{3}{2}} L_0^2 L_y \frac{1}{K_{\frac{n-3}{2}}(\beta)}$$
$$\times \frac{1}{\left[1 + L_0^2 K_x^2 + L_y^2 K_y^2 + L_0^2 K_z^2\right]^{\frac{n}{4}}}$$
$$\times K_{\frac{n}{2}}\left(\beta\left[1 + L_0^2 K_x^2 + L_y^2 K_y^2 + L_0^2 K_z^2\right]^{\frac{1}{2}}\right) \tag{B13}$$

where

$$\beta = \ell_i / L_o. \tag{B14}$$

We have taken the ambient magnetic field direction in the y-direction to more easily transition to the 1-D case employed in this paper. The quantities L_o and L_y are usually referred to as outer scale lengths, with typically

$$L_y \gg L_o. \tag{B15}$$

The quantity ℓ_i is called an inner scale length and is such that

$$\beta \ll 1. \tag{B16}$$

With the PSD given in Eq. B13, we have

$$\Phi_{\delta n}(\mathbf{K}) \sim K^{-n}, \sim \frac{1}{L_0} < K <\sim \frac{1}{\ell_i}. \tag{B17}$$

In general, the axis of symmetry for the electron fluctuation PSD is not related to the platform motion and viewing geometry. For this more general case, the main consequence for the discussions of this work would be to introduce a general positive definite quadratic form to incorporate the decorrelation lengths [cf. Eq. B10] and range and azimuthal effects would become mixed. We here restrict ourselves to the simpler 1-D situation since it contains all the essential elements of the analysis.

As a ray traverses the disturbed ionosphere (here referred to as the z-direction), the phase will acquire a fluctuating contribution, $\delta\phi(\mathbf{r}_\perp)$, [see Eqs. B1 and B2]

$$\delta\phi(\mathbf{r}_\perp) = \lambda r_e \int_{-\ell_p/2}^{\ell_p/2} dz\ \delta n_e(\mathbf{r}_\perp, z) \tag{B18}$$

where ℓ_p is the thickness of the ionosphere. The correla n function for these phase fluctuations is then

$$\left\langle \delta\phi(\mathbf{r}_{\perp 1})\delta\phi(\mathbf{r}_{\perp 2})\right\rangle = \frac{2\pi\beta}{K_{\frac{n-2}{2}}(\beta)}\sigma_\phi^2 \int \frac{d\mathbf{K}_\perp}{(2\pi)^2} e^{i\mathbf{K}_\perp\cdot(\mathbf{r}_1-\mathbf{r}_2)_\perp} \times \frac{L_0 L_y}{\left[1+L_0^2K_x^2+L_y^2K_y^2\right]^{\frac{n}{4}}} K_{\frac{n}{2}}\left(\beta\left[1+L_0^2K_x^2+L_y^2K_y\right]^{\frac{1}{2}}\right), \tag{B19a}$$

or, for $L_y \to \infty$,

$$\left\langle \delta\phi(x_1)\delta\phi(x_2)\right\rangle = \sigma_\phi^2 \frac{(2\pi\beta)^{\frac{1}{2}}}{K_{\frac{n-2}{2}}(\beta)} \int \frac{dK_x}{2\pi} e^{iK_x(x_1-x_2)} \times \frac{L_0}{\left[1+L_0^2K_x^2\right]^{\frac{n-1}{4}}} K_{\frac{n-1}{2}}\left(\beta\left[1+L_0^2K_x^2\right]^{\frac{1}{2}}\right). \tag{B19b}$$

In the above, the average square of the phase fluctuations is

$$\sigma_\phi^2 = \sqrt{2\pi}\lambda^2 r_e^2 \ell_p L_0 \sigma_{Ne}^2 \sqrt{\beta}\frac{K_{\frac{n-2}{2}}(\beta)}{K_{\frac{n-3}{2}}(\beta)}. \tag{B20a}$$

Note that for $n = 4$ and β small, we obtain

$$\sigma_\phi^2 = 2\lambda^2 r_e^2 \ell_p L_0 \sigma_{Ne}^2. \tag{B20b}$$

Above, Eq. B6, we separated the transfer function into a Rayleigh scintillation contribution, h_s, and a phase only contribution. The separation is effected by separating the scale sizes in the phase PSD,

$$\Phi_\phi(K) = \sigma_\phi^2 C(K), \tag{B21a}$$

$$C(K) = \frac{(2\pi\beta)^{\frac{1}{2}}}{K_{\frac{n-2}{2}}(\beta)} \frac{L_0}{\left[1+L_0^2K^2\right]^{\frac{n-1}{4}}} K_{\frac{n-1}{2}}\left(\beta\left[1+L_0^2K^2\right]^{\frac{1}{2}}\right), \tag{B21b}$$

at the Rayleigh wavevector, K_R, determined by the following condition on the Rytov parameter (Ref. 37):

$$0.1 = \sigma_\phi^2 \int_0^{K_R} \frac{dK}{\pi} C(K)\sin^2\gamma L_0^2 K^2 \tag{B22}$$

where

$$\gamma = \frac{R^*\lambda}{4\pi L_0^2}, \tag{B23a}$$

$$R^* = \frac{R_+ R_-}{R_+ + R_-}. \tag{B23b}$$

Clearly, Eq. B22 sets a lower bound for σ_ϕ before Rayleigh scintillations occur. With the typical situation of γ and β being small and for the $n = 4$ PSD, σ_ϕ must satisfy

$$\sigma_\phi^2 > \frac{2}{5\pi}\frac{1}{\gamma} \equiv \sigma_M^2. \tag{B24}$$

A typical value for L_o is

$$L_o = 10 \text{ km} \tag{B25}$$

so for the candidate systems discussed in Section 3, we find

$$\sigma_\phi^2 \text{ (L-band)} > 1970, \tag{B26a}$$

$$\sigma_\phi^2 \text{ (UHF)} > 700. \tag{B26b}$$

(Note that L_y, the outer scale length in the magnetic field direction, is about 150 km.)

The important parameter that characterizes the radar performance is the decorrelation length for the Rayleigh contribution at the radar platform location. The first step is to determine, from Eq. B22, the relationship between σ_ϕ^2 and K_R. Once K_R is determined, the effective decorrelation length satisfies

$$\frac{1}{\ell_0^2} = \frac{1}{2}\left(\frac{R^*}{R_+}\right)^2 \sigma_\phi^2 \int_{K_R}^{\infty} \frac{dK}{\pi} K^2 C(K). \tag{B27}$$

Figure 17 shows the relationship between σ_ϕ and K_R for the two systems discussed in Section 3, again assuming the $n = 4$ PSD, Eq. B25 for L_0 and a value for β of 10^{-3}. The decorrelation length as a function of σ_ϕ is determined from Eq. B27. These relationships for the two systems are shown in Figure 18. Notice that for σ_ϕ/σ_M on the order of unity, the decorrelation length changes very rapidly with $\ell_0 \to \infty$ as $\sigma_\phi/\sigma_M \to 1$. As an example, we will consider severe ambient spread-F. In order to estimate a set of parameters for spread F, we employ the electron density, n_e, measured during PLUMEX I (Ref. 38) and assume locally

$$(\delta n_e)^2 \sim \frac{1}{4} n_e^2.$$

Integration of the experimental data then yields

$$\ell_p \sigma_{Ne}^2 = \int dz\, (\delta n_e)^2 \sim \int dz\, \frac{1}{4} n_e^2 \sim 3.7 \times 10^{28} \text{ m}^{-5}.$$

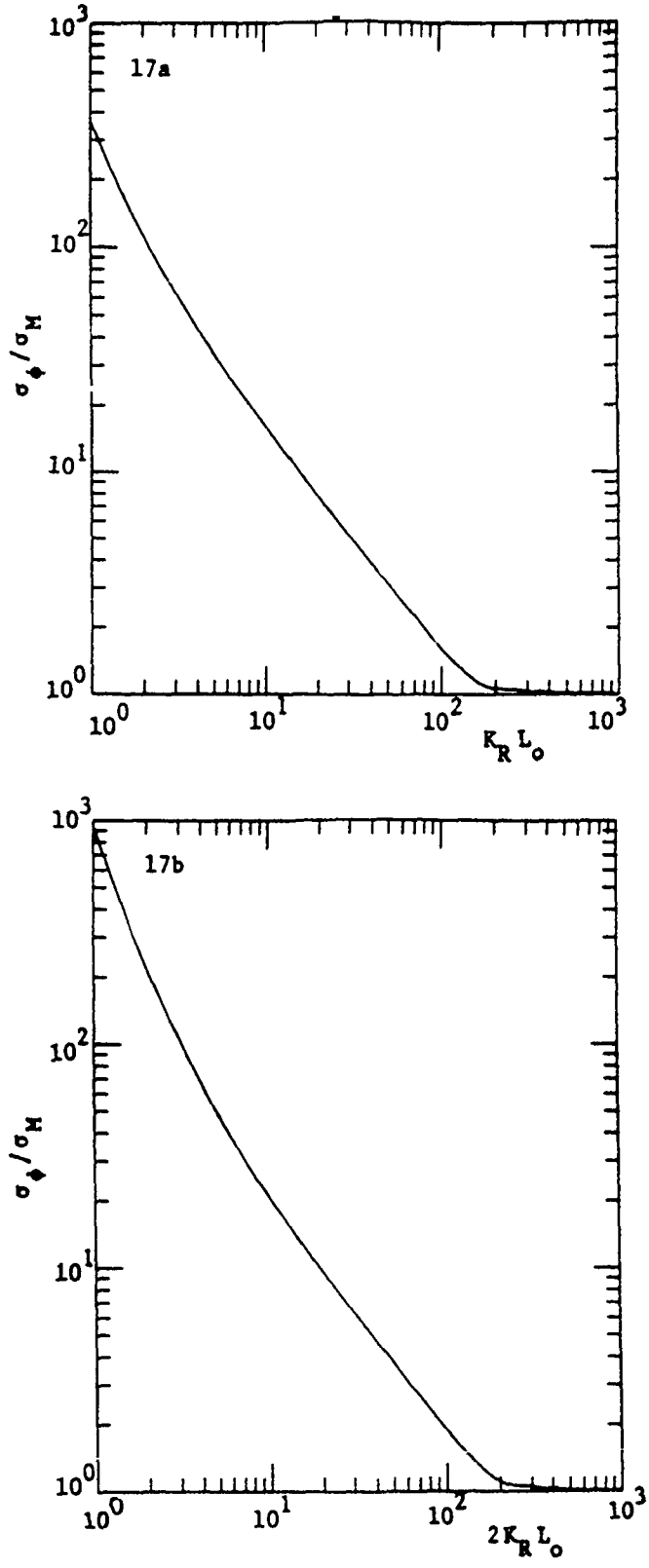

Figure 17. σ_ϕ/σ_M versus $K_R L_0$: a) L-Band, b) UHF.

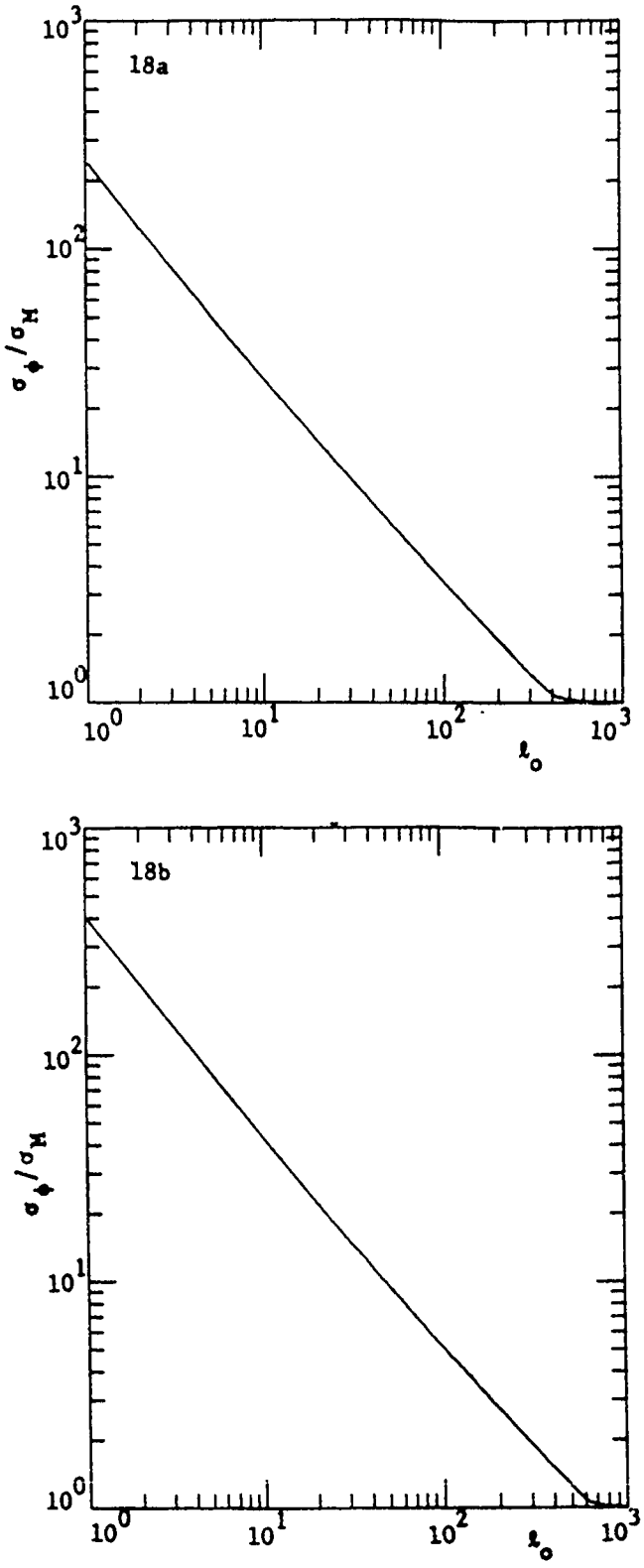

Figure 18. σ_ϕ/σ_M versus ℓ_0: a) L-band, b) UHF.

We then have

$$\sigma_\phi^2 \quad \text{(L-band)} = 368,$$
$$\sigma_\phi^2 \quad \text{(UHF)} = 2880.$$

According to Eq. B26a, the L-band value is lower than that required to produce Rayleigh scintillations. The decorrelation length for the UHF system ($\sigma_\phi/\sigma_M = 2.03$) is found from Figure 18 to be

$$\ell_0 \text{ (UHF)} \sim 250 \text{ m}.$$

We next consider the Doppler spread produced by the long wave-length components of the disturbing media. With Γ, Eq. A34, approximated as in Eq. A51b, we have

$$C_1 = 2T^2V^2\sigma_\phi^2 \int_{\frac{2\pi}{L_S}}^{K_R} \frac{dK}{\pi} K^2 C(K). \tag{B28}$$

The only important effect is in Z_T, Eq. A55. If we define

$$N^2 \frac{Z_T}{\pi} = \beta_1 + \beta_2, \tag{B29a}$$
$$\beta_1 = \frac{2}{\pi} \frac{V_1^2}{S\ell_0^2} t_c^2, \tag{B29b}$$
$$\beta_2 = N^2 \frac{C_1}{\pi}, \tag{B29c}$$

β_1 and β_2 characterize the Doppler spread produced by the Rayleigh scintillations and the long wavelength structure, respectively. As illustrations, Figure 19 shows β_1 and β_2 for the two systems discussed in Section 3, assuming $L_s = Vt_c$. As can be seen, the β_2 contribution is either very small compared to β_1 or both are reasonably small so that the total Doppler spread is quite small.

Finally, we consider the Doppler shift produced by the long wavelength component of the disturbing media. This Doppler shift, δV_D, is given in Eq. A59 as

$$\delta V_D = \frac{\lambda}{2T} \frac{C_2(C) - C_2(T)}{\pi}. \tag{B30}$$

This is a Gaussian random variable with a covariance given by

$$\left\langle (\delta V_D)^2 \right\rangle = \frac{\lambda^2 V^2}{2\pi^2} \left(\frac{R^*}{R_-} \right)^2 \sigma_\phi^2 \int_0^{\widetilde{K}} \frac{dK}{\pi} C(K) K^2 \left[1 - \cos K \frac{R^*}{R_-} X \right] \tag{B31}$$

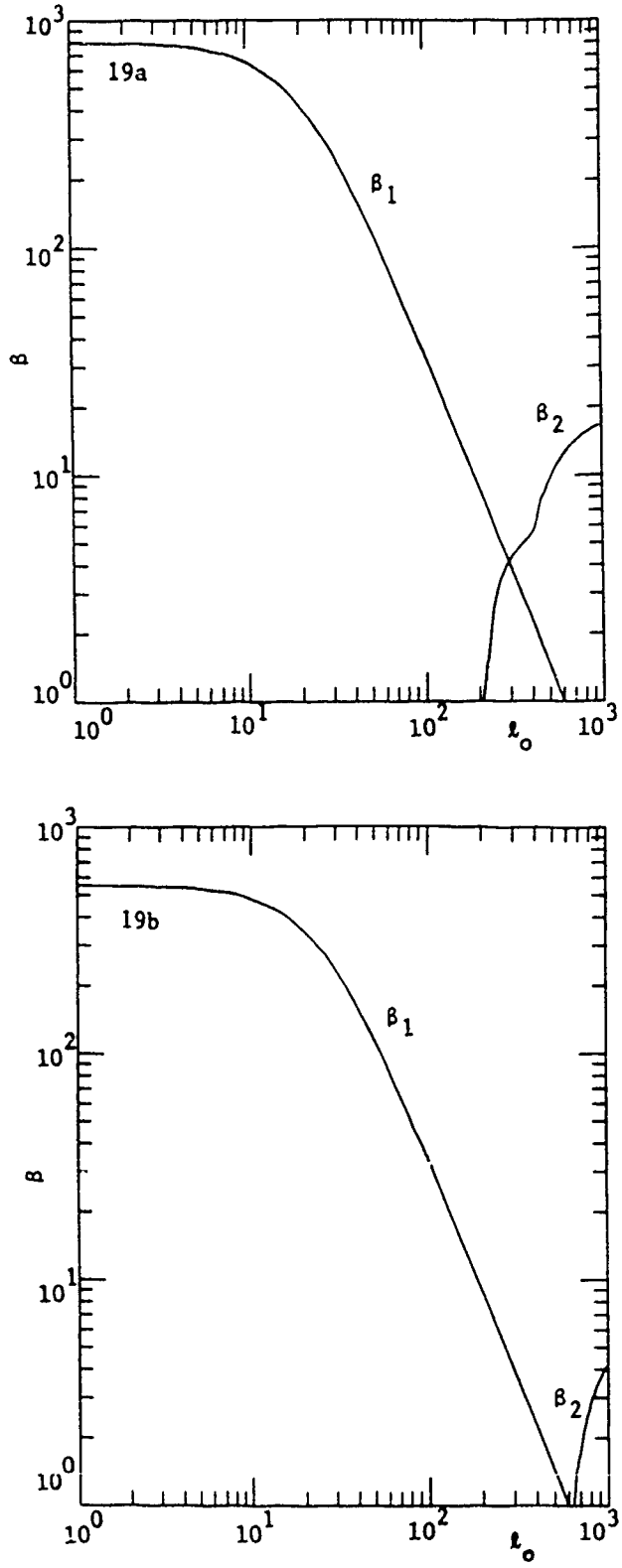

Figure 19. β_1 and β_2 versus ℓ_0: (a) L-band, (b) UHF.

where

$$\tilde{K} = \text{Min}\left(K_R, \frac{2\pi}{L_S}\right) \tag{B34}$$

and X is the separation between the target and the competing clutter. As an illustration of the magnitude of the potential Doppler shift, we will calculate the standard derivation when the separation is the azimuthal extent of the radar footprint, $X = \Delta A$. The results for the two systems discussed in Section 3 are shown in Figure 20. Recall that the ambiguous Doppler velocities ($\lambda/2T$) for the L-band systems are 625 m/sec for the three-phase center approach and 312 m/sec for the two-phase center approach while the corresponding values for the UHF system are 700 m/sec and 350 m/sec, respectively.

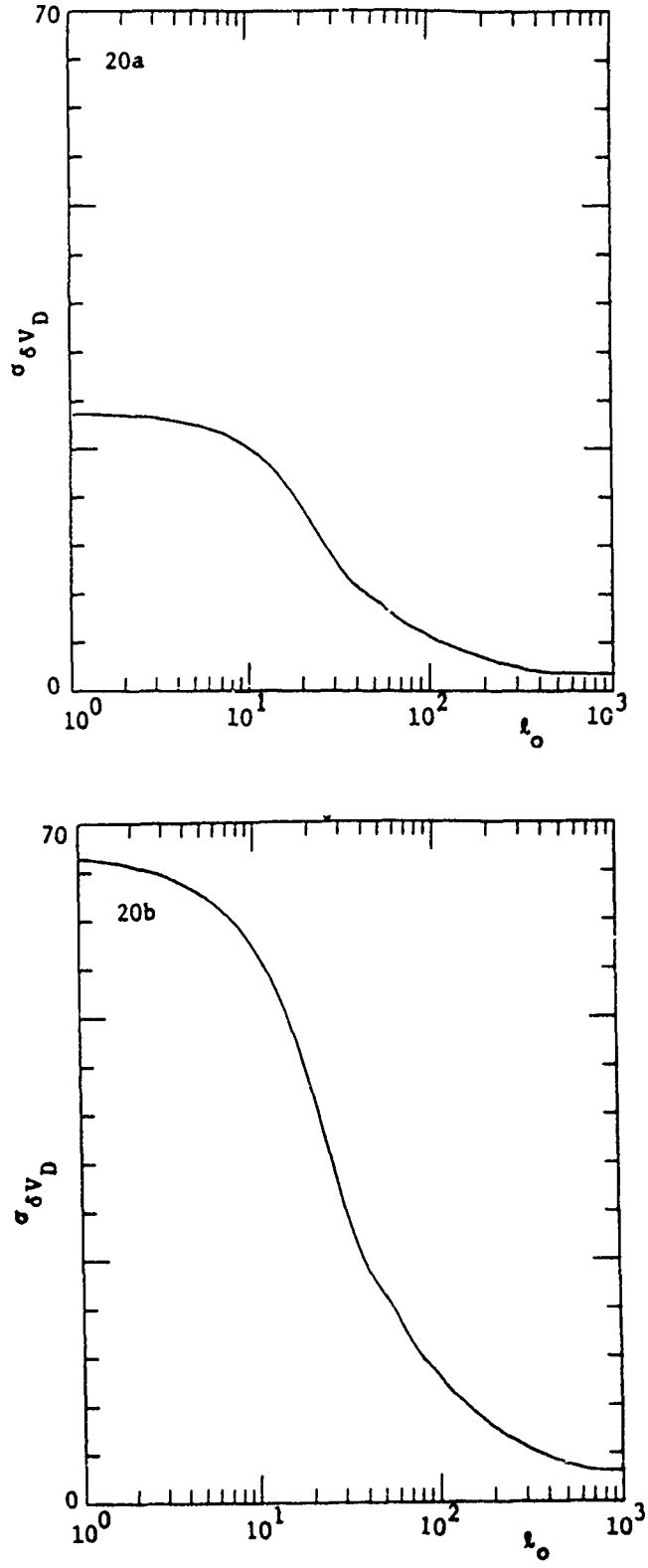

Figure 20. $\sigma_{\delta V_D}$ versus ℓ_0: (a) L-band, (b) UHF.

DISTRIBUTION LIST

DNA-TR-90-78

DEPARTMENT OF DEFENSE

ASSISTANT TO THE SECRETARY OF DEFENSE
ATTN. EXECUTIVE ASSISTANT

DEFENSE ADVANCED RSCH PROJ AGENCY
ATTN. CHIEF SCIENTIST
ATTN: GSD R ALEWINE

DEFENSE COMMUNICATIONS AGENCY
ATTN: C4S/SSM
ATTN: SSS

DEFENSE COMMUNICATIONS ENGINEER CENTER
ATTN: CODE R430 BOEHM

DEFENSE INTELLIGENCE AGENCY
ATTN: DB-TPO
ATTN: DC-6
ATTN: DIR
ATTN DT-1B
ATTN: RTS-2B

DEFENSE NUCLEAR AGENCY
ATTN: NANF
ATTN: NASF
ATTN: OPNA
ATTN: PRPD R YOHO
3 CYS ATTN: RAAE
ATTN: RAAE A CHESLEY
ATTN: RAAE G ULLRICH
ATTN: RAAE K SCHWARTZ
ATTN: RAAE S BERGGREN
ATTN RAEE
2 CYS ATTN TITL

DEFENSE NUCLEAR AGENCY
ATTN: FCPRA LC R HEDTKE
ATTN: TDNM
2 CYS ATTN: TDTT W SUMMA

DEFENSE TECHNICAL INFORMATION CENTER
2 CYS ATTN. DTIC/FDAB

JOINT DATA SYSTEM SUPPORT CTR
ATTN: JNSV

NATIONAL SECURITY AGENCY
ATTN L PLUSWICK

STRATEGIC AND THEATER NUCLEAR FORCES
ATTN DR E SEVIN
ATTN DR SCHNEITER
ATTN. G WINNEBURG

STRATEGIC DEFENSE INITIATIVE ORGANIZATION
ATTN EN
ATTN EN LTC C JOHNSON
ATTN: PTP L STOESSELL
ATTN TN DR M GRIFFIN

THE JOINT STAFF
ATTN: JKC (ATTN: DNA REP)
ATTN: JKCS
ATTN: JLWT THREAT ANALYSIS
ATTN: JPEM

THE JOINT STAFF
ATTN: J6

U S NUCLEAR CMD & CENTRAL SYS SUP STAFF
ATTN: SAB H SEQUINE

DEPARTMENT OF THE ARMY

ARMY LOGISTICS MANAGEMENT CTR
ATTN: DLSIE

HARRY DIAMOND LABORATORIES
ATTN. SLCIS-IM-TL

U S ARMY ATMOSPHERIC SCIENCES LAB
ATTN: SLCAS-AE DR NILES
ATTN: SLCAS-AR DR H HOLT

U S ARMY COMMUNICATIONS R&D COMMAND
ATTN: AMSEL-RD-ESA

U S ARMY ENGINEER DIV HUNTSVILLE
ATTN: PRESTON J KISS

U S ARMY FOREIGN SCIENCE & TECH CTR
ATTN: AIFRTA

U S ARMY MISSILE COMMAND/AMSMI-RD-CS-R
ATTN: AMSMI-RD-CS-R

U S ARMY NUCLEAR & CHEMICAL AGENCY
ATTN. MONA-NU D BASH

U S ARMY NUCLEAR EFFECTS LABORATORY
ATTN: ATAA-PL
ATTN. ATAA-TDC
ATTN: ATRC-WCC LUIS DOMINGUEZ

U S ARMY STRATEGIC DEFENSE CMD
ATTN: CSSD-H-LS B CARRUTH
ATTN: CSSD-H-SA
ATTN: CSSD-H-SAV
ATTN: CSSD-SA-EV RON SMITH

U S ARMY STRATEGIC DEFENSE COMMAND
ATTN. CSSD-GR-S W DICKINSON

USA SURVIVABILITY MANAGMENT OFFICE
ATTN SLCSM-SE J BRAND

DEPARTMENT OF THE NAVY

COMMAND & CONTROL PROGRAMS
ATTN: OP 941

DEPARTMENT OF THE NAVY
ATTN JCMG-707

NAVAL AIR SYSTEMS COMMAND
ATTN PMA 271

NAVAL ELECTRONICS ENGRG ACTVY PACIFIC
ATTN CODE 250

NAVAL RESEARCH LABORATORY
ATTN. CODE 2000 J BROWN
ATTN. CODE 2627
ATTN: CODE 4121.8 H HECKATHORN
ATTN· CODE 4183
ATTN CODE 4701
ATTN: CODE 4720 J DAVIS
ATTN· CODE 4780 B RIPIN
ATTN: CODE 4780 DR P BERNHARDT
ATTN CODE 4780 J HUBA
ATTN CODE 4785 P RODRIGUEZ
ATTN· CODE 5300
ATTN· CODE 5326 G A ANDREWS
ATTN. CODE 5340 E MOKOLE
ATTN: CODE 8344 M KAPLAN
ATTN· JACOB GRUN

NAVAL SURFACE WARFARE CENTER
ATTN· CODE H-21

NAVAL TECHNICAL INTELLIGENCE CTR
ATTN· DA44

NAVAL UNDERWATER SYSTEMS CENTER
ATTN CODE 3411 J KATAN

OFFICE OF CHIEF OF NAVAL OPERATIONS
ATTN. OP 654
ATTN· OP 941D

SPACE & NAVAL WARFARE SYSTEMS CMD
ATTN· CODE 3101 T HUGHES
ATTN PD 50TD
ATTN. PD50TD1 G BRUNHART
ATTN PME 106-4 S KEARNEY
ATTN PME-106 F W DIEDERICH

THEATER NUCLEAR WARFARE PROGRAM OFC
ATTN. PMS-42331F D SMITH

DEPARTMENT OF THE AIR FORCE

AFIA/INKS
ATTN AFIA/INKS MAJ SCHROCK
ATTN AFIA/INKS

AIR FORCE CTR FOR STUDIES & ANALYSIS
ATTN AFCSA/SASC

AIR FORCE ELECTRONIC WARFARE CENTER
ATTN LT M MCNEELY
ATTN SAZ

AIR FORCE OFFICE OF SCIENTIFIC RSCH
ATTN AFOSR/NP

AIR FORCE PHILLIPS LABORATORY
ATTN: J KLOUBACHAR
ATTN OP/W BLUMBERG
ATTN. SANTI BASU

AIR FORCE SYSTEMS COMMAND
ATTN XTTW

AIR FORCE SYSTEMS COMMAND
ATTN. J COLYER

AIR UNIVERSITY LIBRARY
ATTN AUL-LSE

HQ AWS, DET 3 (CSTC/WE)
ATTN WE

NATIONAL TEST FACILITY
ATTN NTB/JPO DR C GIESE

PHILLIPS LABORATORY
ATTN· NTCA
ATTN NTCTS LTC C ROYER
ATTN NTN

STRATEGIC AIR COMMAND/XRFS
ATTN IN
ATTN. XRFS

DEPARTMENT OF ENERGY

EG&G, INC
ATTN D WRIGHT

LAWRENCE LIVERMORE NATIONAL LAB
ATTN· L-97 T DONICH

SANDIA NATIONAL LABORATORIES
ATTN· P L MATTERN 8300

SANDIA NATIONAL LABORATORIES
ATTN. A D THORNBROUGH 400
ATTN CODE 9014 R BACKSTROM
ATTN D DAHLGREN 6410
ATTN DIV 2344 ROBERT M AXLINE
ATTN ORG 9110 G CABLE
ATTN ORG 9110 W D BROWN
ATTN TECH LIB 3141

OTHER GOVERNMENT

CENTRAL INTELLIGENCE AGENCY
ATTN. OSWR/NED
ATTN OSWR/SSD FOR L BERG

DEPARTMENT OF COMMERCE
ATTN· G REEVE
ATTN J HOFFMEYER
ATTN W UTLAUT

U S DEPARTMENT OF STATE
ATTN PM/TMP

DEPARTMENT OF DEFENSE CONTRACTORS

AEROSPACE CORP
ATTN A MORSE
ATTN. BRIAN PURCELL
ATTN: C CREWS 92957
ATTN: C RICE
ATTN DR J M STRAUS
ATTN. G LIGHT
ATTN: I GARFUNKEL
ATTN: J KLUCK
ATTN. J THACKER
ATTN M ROLENZ

AT&T BELL LABORATORIES
ATTN: DENIS S LONGO
ATTN: JOSEPH A SCHOLL
ATTN: N BEAUCHAMP

ATLANTIC RESEARCH SERVICES CORP
ATTN: R MCMILLAN

ATMOSPHERIC AND ENVIRONMENTAL RESEARCH INC
ATTN M KO

AUSTIN RESEARCH ASSOCIATES
ATTN. J THOMPSON

AUTOMETRIC, INC
ATTN. C LUCAS

BDM INTERNATIONAL INC
ATTN. W LARRY JOHNSON

BERKELEY RSCH ASSOCIATES, INC
ATTN. J WORKMAN
ATTN: N T GLADD
ATTN: S BRECHT

BOEING CO
ATTN: G HALL

CALIFORNIA RESEARCH & TECHNOLOGY, INC
ATTN. M ROSENBLATT

CHARLES STARK DRAPER LAB, INC
ATTN. A TETEWSKI

COMMUNICATIONS SATELLITE CORP
ATTN RICHARD A ARNDT

CONTEL FEDERAL SYSTEMS INC
ATTN. CHARLES BENNINGTON

CORNELL UNIVERSITY
ATTN: D FARLEY JR
ATTN M KELLY

DYNETICS, INC
ATT J: WILLIAM D TEPPER

ELECTROSPACE SYSTEMS, INC
ATTN: LINDA CALDWELL
ATTN P PHILLIPS

EOS TECHNOLOGIES, INC
ATTN. B GABBARD
ATTN: R LELEVIER

FORD AEROSPACE CORPORATION
ATTN: PATRICIA BIRDWELL

GENERAL ELECTRIC COMPANY
ATTN JOSEPH E STROSSER

GENERAL RESEARCH CORP INC
ATTN: J EOLL

GRUMMAN AEROSPACE CORP
ATTN: J DIGLIO

HARRIS CORPORATION
ATTN: LYMUEL MCRAE

HSS, INC
ATTN. D HANSEN

INFORMATION SCIENCE, INC
ATTN: W DUDZIAK

INSTITUTE FOR DEFENSE ANALYSES
ATTN. E BAUER
ATTN. H WOLFHARD

JAYCOR
ATTN: A GLASSMAN
ATTN: J SPERLING

JOHNS HOPKINS UNIVERSITY
ATTN. C MENG
ATTN: H G TORNATORE
ATTN: J D PHILLIPS
ATTN R STOKES

KAMAN SCIENCES CORP
ATTN: DASIAC
ATTN. E CONRAD
ATTN: G DITTBERNER

KAMAN SCIENCES CORPORATION
ATTN: B GAMBILL
ATTN: DASIAC
ATTN R RUTHERFORD

LOCKHEED MISSILES & SPACE CO, INC
ATTN: J HENLEY
ATTN: J KUMER
ATTN R SEARS

LOCKHEED MISSILES & SPACE CO, INC
ATTN. CARL CRABILL
ATTN: D T RAMPTON
ATTN. E M DIMZCELI

LTV AEROSPACE & DEFENSE COMPANY
2 CYS ATTN. LIBRARY EM-08

M I T LINCOLN LAB
ATTN: D TOWLE L-230
ATTN. I KUPIEC L-100

MARTIN MARIETTA DENVER AEROSPACE
ATTN: J BENNETT
ATTN: H VON STRUVE III

MAXIM TECHNOLOGIES, INC
ATTN: B PHILLIPS
ATTN: N CIANOS

MAXWELL LABS, INC
ATTN: K WARE

MCDONNELL DOUGLAS CORPORATION
ATTN: J GROSSMAN
ATTN: R HALPRIN

METATECH CORPORATION
ATTN: W RADASKY

METEOR COMMUNICATIONS CORP
ATTN: R LEADER

MISSION RESEARCH CORP
ATTN: R ARMSTRONG
ATTN: W WHITE

MISSION RESEARCH CORP
ATTN: R L BOGUSCH

MISSION RESEARCH CORP
ATTN: DAVE GUICE

MISSION RESEARCH CORP
ATTN: B R MILNER
ATTN: C LONGMIRE
ATTN: D KNEPP
ATTN: D LANDMAN
ATTN: F FAJEN
ATTN: F GUIGLIANO
ATTN. G MCCARTOR
ATTN: K COSNER
ATTN: M FIRESTONE
ATTN. R BIGONI
ATTN: R DANA
ATTN: R HENDRICK
ATTN: R KILB
ATTN: S GUTSCHE
ATTN: TECH LIBRARY

MITRE CORPORATION
ATTN. M HORROCKS
ATTN: R C PESCI W-34
ATTN: W FOSTER

MITRE CORPORATION
ATTN: G CAMPARETTO

NORTHWEST RESEARCH ASSOC, INC
ATTN: E FREMOUW

PACIFIC-SIERRA RESEARCH CORP
ATTN: E FIELD JR
ATTN: H BRODE

PHOTOMETRICS, INC
ATTN: I L KOFSKY

PHOTON RESEARCH ASSOCIATES
ATTN: D BURWELL

PHYSICAL RESEARCH INC
ATTN: W SHIH

PHYSICAL RESEARCH INC
ATTN: A CECERE

PHYSICAL RESEARCH INC
ATTN: H FITZ

PHYSICAL RESEARCH, INC
ATTN: R DELIBERIS
ATTN: T STEPHENS

PHYSICAL RESEARCH, INC
ATTN: J DEVORE
ATTN: J THOMPSON
ATTN. W SCHLUETER

PHYSICS INTERNATIONAL CO
ATTN: C GILMAN

R & D ASSOCIATES
2 CYS ATTN: B LAMB
ATTN: G HOYT
5 CYS ATTN: L DEREAD

R & D ASSOCIATES
ATTN: D CARLSON
ATTN J THOMPSON

RAND CORP
ATTN: C CRAIN
ATTN: E BEDROSIAN

RAND CORP
ATTN: B BENNETT

RJO ENTERPRISES/POET FAC
ATTN. STEVEN KRAMER

ROCKWELL INTERNATIONAL CORP
ATTN: R POTTER

SCIENCE APPLICATIONS INTL CORP
ATTN: C SMITH
ATTN: D SACHS
ATTN. L LINSON

SCIENCE APPLICATIONS INTL CORP
ATTN: H SUNKENBERG
ATTN: LIBRARY

SCIENCE APPLICATIONS INTL CORP
ATTN: S ROSENCWEIG

SPARTA INC
ATTN: D DEAN

SRI INTERNATIONAL
ATTN: R LIVINGSTON
ATTN: R T TSUNODA
ATTN: W CHESNUT
ATTN: W JAYE

STEWART RADIANCE LABORATORY
ATTN: R HUPPI

TELECOMMUNICATION SCIENCE ASSOCIATES
ATTN: R BUCKNER

TELEDYNE BROWN ENGINEERING
ATTN: J FORD
ATTN: J WOLFSBERGER JR
ATTN: N PASSINO

TOYON RESEARCH CORP
ATTN: J ISE

TRW INC
ATTN: ED SIMMONS

TRW SPACE & DEFENSE SECTOR SPACE &
ATTN: D M LAYTON

USER SYSTEMS, INC
ATTN: S W MCCANDLESS JR

UTAH STATE UNIVERSITY
ATTN: K BAKER
ATTN: L JENSEN

VISIDYNE, INC
ATTN: J CARPENTER

FOREIGN

FOA 2
ATTN: B SJOHOLM

DIRECTORY OF OTHER

BOSTON UNIVERSITY
ATTN: MICHAEL MENDILLO